Title

The effect mitigation measures for COVID-19 by a fractional-order SEIHRDP model with individuals migration

Authors

Lu, Zhenzhen
Chen, YangQuan
Yu, Yongguang
et al.

Publication Date

2023

DOI

10.1016/j.isatra.2022.12.006

Peer reviewed

Since January 2020 Elsevier has created a COVID-19 resource centre with free information in English and Mandarin on the novel coronavirus COVID-19. The COVID-19 resource centre is hosted on Elsevier Connect, the company's public news and information website.

ISA Transactions 132 (2023) 582–597

Contents lists available at ScienceDirect

ISA Transactions

journal homepage: www.elsevier.com/locate/isatrans

The effect mitigation measures for COVID-19 by a fractional-order SEIHRDP model with individuals migration

Zhenzhen Lu [a], YangQuan Chen [b], Yongguang Yu [a,*], Guojian Ren [a], Conghui Xu [a], Weiyuan Ma [c], Xiangyun Meng [a]

[a] Department of Mathematics, Beijing Jiaotong University, Beijing, 100044, PR China
[b] Mechatronics, Embedded Systems and Automation Lab, University of California, Merced, CA 95343, USA
[c] School of Mathematics and Computer Science, Northwest Minzu University, Lanzhou, 730000, PR China

ARTICLE INFO

Article history:
Received 5 August 2020
Received in revised form 22 November 2022
Accepted 10 December 2022
Available online 14 December 2022

Keywords:
Individual migration
Fractional-order epidemic model
Peak prediction
Sensitivity

ABSTRACT

In this paper, the generalized SEIHRDP (susceptible–exposed–infective–hospitalized–recovered–death–insusceptible) fractional-order epidemic model is established with individual migration. Firstly, the global properties of the proposed system are studied. Particularly, the sensitivity of parameters to the basic reproduction number are analyzed both theoretically and numerically. Secondly, according to the real data in India and Brazil, it can all be concluded that the bilinear incidence rate has a better description of COVID-19 transmission. Meanwhile, multi-peak situation is considered in China, and it is shown that the proposed system can better predict the next peak. Finally, taking individual migration between Los Angeles and New York as an example, the spread of COVID-19 between cities can be effectively controlled by limiting individual movement, enhancing nucleic acid testing and reducing individual contact.

1. Introduction

End of 2019 saw the outbreak of the dangerous infectious disease COVID-19, which is brought on by a novel coronavirus. Global public health has been significantly impacted by the 13,837,395 diagnosed cases and the 590,702 death cases as of July 17, 2020 [1]. The quick rise in infection cases suggests that COVID-19 has a much greater ability to spread than MERS-CoV and SARS coronaviruses [2,3]. A direction for taking the right steps can be provided by a deeper comprehension and insight of the epidemic tendencies. Numerous nations have implemented a variety of mitigating strategies to prevent the spread of COVID-19 since 23 January, 2020. These strategies include home isolation, herd immunity, limiting individual migration, and others.

Lack of information on the dynamic mechanism relating to the severity of COVID-19 at the this early stage makes it extremely difficult to limit the spread of COVID-19. However, using a mathematical model, strategies can be measured to serve as a benchmark for determining whether mitigation strategies are adequate. During the modeling process, it is very important to describe how infectious diseases are transmitted between susceptible and infected individuals. Numerous studies have shown that the incidence rate, which measures the infection capacity of a single infected person per unit time, is a crucial tool for describing this process, where susceptible individuals come into contact with infected individuals and are then infected with such a predetermined probability [4–7]. Meanwhile, Korobeinikov et al. [8] indicated that the stability of the endemic equilibrium point is closely related to the concave of the incidence rate with respect to the infected individuals. Therefore, many researchers established the epidemic model of COVID-19 under various incidence rates [9–11], for example, Peng et al. [9] constructed the SEIR (E-exposed) epidemic model and they discovered that COVID-19's first appearance might be traced to the end of December 2019. A SEIQRD (Q-diagnosed) model was taken into consideration by Xu et al. [10], which has some basic guiding relevance for predicting COVID-19.

Besides, individual migration has a crucial effect on the evolution of infectious diseases. With the convenience between cities, individuals move more and more frequent and new infectious diseases develop more rapidly regionally and globally [12]. Numerous deterministic models with multiple patches have been presented in attempt to better understand how individual migration affects the spread of infectious illnesses [13–15]. Contrary to what was initially reported [16], COVID-19 is in fact spreading from person to person through continuous interpersonal contact [2]. Lu et al. [17] considered a fractional-order SEIHRD (H-hospitalized) model with inter-city networks and they found that COVID-19 could be reduced in low-risk areas, but increased

* Corresponding author.
E-mail address: ygyu@bjtu.edu.cn (Y. Yu).

https://doi.org/10.1016/j.isatra.2022.12.006
0019-0578/

in high-risk areas by restricting communication between cities. Meanwhile, cross-infection among cities are considered, while there is not consider for self-migration [17]. Therefore, it is of great practical significance to include individual migration in different cities or different countries with the modeling COVID-19. Furthermore, the migration of susceptible, exposed, infected individuals are studied in this paper.

It is worth noting that the time which patients waits for treatment follows the power law distribution [18], which prompts the use of the Caputo fractional-order derivative [19]. Angstmann et al. [20] discovered how fractional operators naturally appear in their model if the recovery time is a power law distribution after building a SIR epidemic model. Meanwhile, this offers a chronic disease epidemic model in which long-term infected people have little chance of recovering. Based on this statement, several authors have stated that the fractional-order model plays an important role in the process of disease transmission. Khan et al. [21] recounted how individuals, bats, unidentified hosts, and the source of the illness interacted, and considered how crucial the fractional-order system was in preventing the spread of the infection. To predict the spread of COVID-19, Chen et al. [22] developed a fractional-order epidemic model. Amjad et al. [23] built a fractional-order COVID-19 model and calculated the consequences of several mitigation and prevention strategies.

Motivated by the above discussion, a fractional-order SEIHRDP epidemic model with individuals movement is established in this paper to study COVID-19. Meanwhile, the number of hospitalizations is the same as confirmed isolation in China, and but in other countries, these two are not equal, which the number of confirmed case is greater than that of hospitalized case. So in order to give a more generalized model, the purpose of this paper is to describe hospitalized individuals in response to the spread of COVID-19. The infectiousness of the incubation time is also taken into consideration, as inspired by [24]. Then, the proposed system's dynamic behaviors are investigated, including the existence and uniqueness of the nonnegative solution, the global asymptotic stability of the disease-free equilibrium, and the uniform persistence, all of which have theoretical implications for future COVID-19 intervention and prevention. Meanwhile, the basic reproduction number with and without individual migration are compared, and it is found that adding individual migration can effectively describe the spread of COVID-19. Furthermore, the sensitivity of parameters to the basic reproduction number are analyzed both theoretically and numerically. Meanwhile, considering India and Brazil, results suggest that the bilinear incidence rate may be more fitted than the saturation incidence rate for stimulating the spread of COVID-19. When individuals movement is not considered, it can be found the proposed fractional-order model can better predict than the integer-order for multi peaks of COVID-19 in China. Meanwhile, when individuals movement is considered, the epidemic in the United States is analyzed and some mitigation measures are carried out to control the development of COVID-19. An implication of the achieved results is the possibility that the United States peaked on 24 November, 2020 (integer-order system) and 1 January, 2021 (fractional-order system), however, the number of infections shows an downward trend after 17 July, 2020 as enhancing nucleic acid detection and reducing the contact rate. Meanwhile, considering measures to limit migration between New York and Los Angeles, and enhance nucleic acid detection and reduce exposure rates, it is evident that there is an immediate increase in confirmed cases before a drop.

Based on the above analysis, a generalized fractional-order SEIHRDP epidemic model with individual migration is considered. The main contributions of this study are as follows:

- A fractional-order epidemic model with self-migration is considered, in which the infectivity of exposed individuals and hospitalized individuals are also taken into account.
- The global properties of the proposed model are investigated, including the existence and uniqueness of global positive solutions, the local and global stability of disease-free equilibrium points, the persistence of disease transmission.
- The sensitivity of parameters to the basic reproduction number are analyzed both theoretically and numerically.
- Based on real data, the impact of the incidence rate on modeling COVID-19 is studied in India and Brazil.
- Multiple peaks of COVID-19 transmission in China are analyzed by the proposed system.
- Individual movement in the spread of COVID-19 in the United States is investigated and the peak are analyzed based on mitigation measures, such as enhanced nucleic acid testing, reduced of individual exposure, and control of individual movement.

The rest of this paper is organized as follows. The SEIHRDP fractional-order model with individual movement is developed for COVID-19 in Section 2 and provides some preliminaries. Then dynamic properties of the proposed system are examined in Section 3. The theoretical results are shown using numerical simulations in Section 4. Finally, Section 5 provides the conclusions.

2. System description and preliminaries

Fractional-order operator have been determined to have a wide range of uses in the modeling of many dynamic processes, including those in engineering, biology, medicine, and others [25–28]. In this part, some necessary preliminaries are introduced before the fractional-order epidemic model is presented.

2.1. Preliminaries

Definition 2.1 ([29]). The Caputo fractional-order operator is defined by

$$
\begin{aligned}
{}_0^C D_t^\alpha g(t) &= \frac{d^\alpha g(t)}{dt^\alpha} \\
&= \frac{1}{\Gamma(n-\alpha)} \int_0^t \frac{g^{(n)}(s)}{(t-s)^{\alpha-n+1}} ds, (n-1 < \alpha < n),
\end{aligned}
$$

where $g^{(n)}(s)$ is the nth derivative of $g(s)$ with respect to s.

Remark 2.1. If $\alpha = n$, one has

$${}_0^C D_t^\alpha g(t) = g^{(n)}(t).$$

Lemma 2.1 ([30]). *The Caputo nonlinear system is considered as follows:*

$${}_0^C D_t^\alpha x(t) = g(x), (\alpha \in (0, 1]),$$

with the initial condition x_0. If all eigenvalues of $J|_{x=x^*} = \frac{\partial g}{\partial x}|_{x=x^*}$ satisfy $|arg(\lambda)| > \frac{\alpha\pi}{2}$, the equilibrium points x^* are locally asymptotically stable.

Lemma 2.2 ([31]). *Suppose $\mathbb{X} \subset \mathbb{R}$ and the continuous operator $T(t) : \mathbb{X} \to \mathbb{X}$ satisfies*
(1) $T(t)$ is point dissipative in $\mathbb{X}$ and compact for $t \geq 0$.
(2) there is a finite sequence $M = \{M_1, M_2, \ldots, M_k\}$ of compact and isolated invariant sets such that
(i) $M_i \cap M_j = \emptyset$ for any $i, j = 1, 2, \ldots, k$ and $i \neq j$;
(ii) $\Omega(\partial X^0) \triangleq \cup_{x \in \partial X^0} \omega(x) \subset \cup_{i=1}^k M_i$;
(iii) in the case of $\partial \mathbb{X}^0$, no a cycle is formed by any subset of M;
(iv) $W^s(M_i) \cap \mathbb{X}^0 = \emptyset$ for each $i = 1, 2, \ldots, k$.
Then $T(t)$ is uniformly persistent in $\mathbb{X}$.

2.2. Graph theory

In this paper, a weighted graph $\zeta = (\vartheta, \omega, A)$ will be considered to model the spread of infectious diseases between cities, where $\vartheta = \{\vartheta_1, \vartheta_2, \ldots, \vartheta_n\}$ denotes the node set and ϑ_i represents the ith city; $\omega \subseteq \vartheta \times \vartheta$ is the edge set, and if there is individual movement between any two cities, it means that there is a edge between this two cities; matrixes $M = [m_{ij}]_{1\le i,j\le n}$, $N = [n_{ij}]_{1\le i,j\le n}$, $P = [p_{ij}]_{1\le i,j\le n}$ and $Q = [q_{ij}]_{1\le i,j\le n}$ represent the weighted adjacency matrix of susceptible, exposed, infected and recovered individual, respectively; m_{ij}, n_{ij}, p_{ij} and q_{ij} denote the migrate rate of susceptible, exposed, infected and recovered individual from city j to city i with $a_{ij} \ge 0$ $(i \ne j)$ and $a_{ii} = 0$ $(a = m, n, p \text{ or } q)$, respectively. Furthermore, based on the directivity of individual migration, the directed graph ζ is studied in this paper.

2.3. System description

Starting from 23 January, 2020, the Chinese government has adopted a series of mitigation measures to effectively suppress the spread of COVID-19, such as implementing strict home isolation, restricting various traffic, strengthening nucleic acid testing, establishing shelter hospitals and so on. Meanwhile, other countries around the world have adopted different measures from China, such as social distancing and herd community strategy by British, protecting sensitive compartment from infection by Italy, transferring of critically ill patients with military aircraft by France, etc. Therefore, it is important to establish a generalized model of individual migration to simultaneously quantify the impact of interruption of policies on virus transmission. Moreover, Tang et al. [32] proposed that the exposed individual is infectious of COVID-19. Therefore, a fractional-order SEIHRDP epidemic model with individual migration is considered as follows:

$$\begin{cases} {}_0^C D_t^\alpha S_k = \Lambda_k - \beta_{1k} S_k f_k(I_k) - \beta_{2k} S_k g_k(E_k) - \rho_k S_k \\ \qquad\qquad + \sum_{j=1}^{n} (m_{kj} S_j - m_{jk} S_k), \\ {}_0^C D_t^\alpha E_k = \beta_{1k} S_k f_k(I_k) + \beta_{2k} S_k g_k(E_k) - \epsilon_k E_k \\ \qquad\qquad + \sum_{j=1}^{n} (n_{kj} E_j - n_{jk} E_k), \\ {}_0^C D_t^\alpha I_k = \epsilon_k E_k - \delta_k I_k + \sum_{j=1}^{n} (p_{kj} I_j - p_{jk} I_k), \\ {}_0^C D_t^\alpha H_k = \delta_k I_k - (\lambda_k + \kappa_k) H_k, \\ {}_0^C D_t^\alpha R_k = \lambda_k H_k + \sum_{j=1}^{n} (q_{kj} R_j - q_{jk} R_k), \\ {}_0^C D_t^\alpha D_k = \kappa_k H_k, \\ {}_0^C D_t^\alpha P_k = \rho_k S_k. \end{cases} \tag{1}$$

with the initial condition

$$S_k(0) = S_{k0} > 0, \quad E_k(0) = E_{k0} \ge 0, \quad I_k(0) = I_{k0} \ge 0, \quad H_k(0) = H_{k0} \ge 0,$$
$$R_k(0) = R_{k0} \ge 0, \quad D_k(0) = D_{k0} \ge 0, \quad P_k(0) = P_{k0} \ge 0. \tag{2}$$

The specific explanation of system (1) are as follows:

- Susceptible S_k: the number of susceptible class within city k at time t.
- Exposed E_k: the number of exposed class within city k at time t (neither any clinical symptoms nor high infectivity).
- Infectious I_k: the number of infected class within city k at time t (with overt symptoms).
- Hospitalized H_k: the number of hospitalized class within city k at time t.
- Recovered R_k: the number of recovered class within city k at time t.
- Dead D_k: the number of dead class within city k at time t.
- Insusceptible P_k: the number of susceptible class who are not exposed to the external community within city k at time t.

Meanwhile, the process of disease transmission are as follows:

- The susceptible individual S_k contacts with E_k and I_k, and then is infected by $\beta_{1k} S_k f_k(I_k) + \beta_{2k} S_k g_k(E_k)$, where β_{ik} $(i = 1, 2)$ are the transmission coefficient, $f_k(I_k)$ and $g_k(E_k)$ are generalized incidence rates.
- The parameter Λ_k is the inflow rate; λ_k, ϵ_k, δ_k and κ_k represent the recovery, incubation, diagnosis, mortality rate.
- The susceptible, exposed, infective and recovered individuals in city j move to city k with probability m_{kj}, n_{kj}, p_{kj} and q_{kj}, respectively. The terms $\sum_{j=1}^{n}(m_{kj}S_j - m_{jk}S_k)$, $\sum_{j=1}^{n}(n_{kj}E_j - n_{jk}E_k)$, $\sum_{j=1}^{n}(p_{kj}I_j - p_{jk}I_k)$ and $\sum_{j=1}^{n}(q_{kj}R_j - q_{jk}R_k)$ represent the movement of S_k, E_k I_k and R_k individual, where $\sum_{j=1}^{n} a_{kj}W_j$ represents the individuals moving into k city from other cities j $(k \ne j)$ and $\sum_{j=1}^{n} a_{jk}W_j$ represents the individuals leaving city k $(W = S, E, I, R$, respectively, $a = m, n, p, q$, respectively).
- The movement of insusceptible and hospitalized individuals is not considered in this paper.

Furthermore, Λ_k, β_{ik} $(i = 1, 2)$, ρ_k and ϵ_k are positive constants; functions $\delta_k(t)$, $\lambda_k(t)$, $\kappa_k(t)$, $m_{kj}(t)$, $n_{kj}(t)$, $p_{kj}(t)$ and $q_{kj}(t)$ satisfy $|\delta_k(t)| \le M_{1k}$, $|\lambda_k(t)| \le M_{2k}$, $|\kappa_k(t)| \le M_{3k}$, $|m_{kj}(t)| \le M_{4k}$, $|n_{kj}(t)| \le M_{5k}$, $|p_{kj}(t)| \le M_{6k}$ and $|q_{kj}(t)| \le M_{7k}$ for all $t \ge 0$ and $k, j = 1, 2, \ldots, n$, where M_{1k}, M_{2k}, M_{3k}, M_{4k}, M_{5k}, M_{6k} and M_{7k} are positive constants. The transmission diagram of the generalized SEIHRDP model (1) is shown in Fig. 1.

Before presenting the major findings, the following generalized incidence rate hypothesis is put forth:

(**H**): (*i*) $g_k(E_k)$ *and* $f_k(I_k)$ *satisfy the local Lipschitz condition and* $g_k(0) = 0, f_k(0) = 0$ *for* $k = 1, 2, \ldots, n$;
(*ii*) $f_k(I_k)$ *is strictly monotone increasing on* $I_k \in [0, \infty)$ *and* $g_k(E_k)$ *is strictly monotone increasing on* $E_k \in [0, \infty)$ *for all* $k = 1, 2, \ldots, n$;
(*iii*) $f_k(I_k) \le a_k I_k$ *for all* $I_k \ge 0$, *where* $a_k = f_k'(0)$ *for all* $k = 1, 2, \ldots, n$;
(*iv*) $g_k(E_k) \le b_k E_k$ *for all* $E_k \ge 0$, *where* $b_k = g_k'(0)$ *for all* $k = 1, 2, \ldots, n$.

Remark 2.2. It should be noted that many current models can be viewed as a special type of system (1) with the hypothesis (**H**), such as $g_k(E_k) = b_k E_k$, $g_k(E_k) = \frac{b_k E_k}{1+v_k E_k}$, $f_k(I_k) = a_k I_k$, $f_k(I_k) = \frac{a_k I_k}{1+u_k I_k}$ and others [33] with nonnegative constants a_k, b_k, u_k and v_k.

Remark 2.3. Compared with [34], the individual movement in this paper can be described as follows:
(1) the self-migration of individuals is described in system (1), which is caused by a self-chemotactic-like forcing [35]. However, the cross-infection among cities is considered which is a travel infectious [34].
(2) system (1) describes not only the migration of infected individuals, but also the movement of exposed and recovered individuals.
(3) $M = [m_{ij}]_{1\le i,j\le n}$, $N = [n_{ij}]_{1\le i,j\le n}$, $P = [p_{ij}]_{1\le i,j\le n}$ and $Q = [q_{ij}]_{1\le i,j\le n}$ are not irreducible in this paper, but irreducible

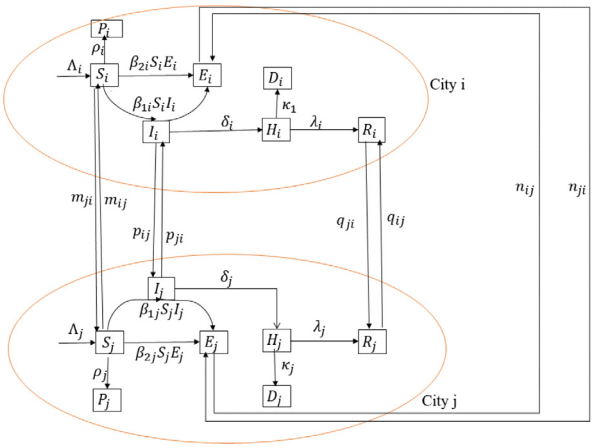

Fig. 1. The schematic diagram of SEIHRDP epidemic model with individual migration $(i, j = 1, 2, \ldots, n)$.

in [34]. Then the influence of network structure on disease transmission can be discussed in this paper, such as fully connected network, ring network and centralized network. However, [34] only consider fully connected network.
(4) the total population of each city is changed (without considering the decrease in population due to death) in system (1). But in [34], the total population of each city remains constant.

3. System analysis

This study explores system (1)'s dynamic analysis. As can be seen, the death class D_k and the insusceptible class P_k have no effect on the susceptible class S_k, exposed class E_k, infected class I_k, hospitalized class H_k, or recovered class R_k of systems (1). Accordingly, the following system is discussed in the next section:

$$\begin{cases} {}_0^C D_t^\alpha S_k = \Lambda_k - \beta_{1k} S_k f_k(I_k) - \beta_{2k} S_k g_k(E_k) - \rho_k S_k \\ \qquad + \sum_{j=1}^{n} (m_{kj} S_j - m_{jk} S_k), \\ {}_0^C D_t^\alpha E_k = \beta_{1k} S_k f_k(I_k) + \beta_{2k} S_k g_k(E_k) - \epsilon_k E_k \\ \qquad + \sum_{j=1}^{n} (n_{kj} E_j - n_{jk} E_k), \\ {}_0^C D_t^\alpha I_k = \epsilon_k E_k - \delta_k I_k + \sum_{j=1}^{n} (p_{kj} I_j - p_{jk} I_k), \\ {}_0^C D_t^\alpha H_k = \delta_k I_k - (\lambda_k + \kappa_k) H_k, \\ {}_0^C D_t^\alpha R_k = \lambda_k H_k + \sum_{j=1}^{n} (q_{kj} R_j - q_{jk} R_k), \end{cases} \tag{3}$$

with the initial condition

$$\begin{aligned} &S_k(0) = S_{k0} > 0, \quad E_k(0) = E_{k0} \geq 0, \quad I_k(0) = I_{k0} \geq 0, \\ &H_k(0) = H_{k0} \geq 0, \quad R_k(0) = R_{k0} \geq 0, \ (k = 1, 2, \ldots, n). \end{aligned} \tag{4}$$

3.1. Existence and uniqueness of the positive solution

The existence, uniqueness, and boundedness of the nonnegative solution for system (3) should be taken into account prior to the numerical process. Therefore, this subsection will be discussed these properties for system (3).

Theorem 3.1. *For any nonnegative initial condition (4), there are a unique solution for system (3) and the region*

$$\begin{aligned} \Omega = \{&(S_1, E_1, I_1, H_1, R_1, \ldots, S_n, E_n, I_n, H_n, R_n) : \\ &0 < S_i \leq \frac{\Lambda}{\rho}, 0 \leq E_i \leq \frac{\Lambda}{\rho}, 0 \leq I_i \leq \frac{\Lambda}{\rho}, \\ &0 \leq H_i \leq \frac{\Lambda}{\rho}, 0 \leq R_i \leq \frac{\Lambda}{\rho}, i = 1, 2, \ldots, n\} \end{aligned}$$

is positively invariant for system (3), where $\Lambda = \sum_{j=1}^{n} \Lambda_j$ *and* $\rho = \min\{\rho_1, \rho_2, \ldots, \rho_n\}$.

Proof. Let consider the following function:

$$\begin{cases} f_{1k} = \Lambda_k - \beta_{1k} S_k f_k(I_k) - \beta_{2k} S_k g_k(E_k) - \rho_k S_k \\ \qquad + \sum_{j=1}^{n} (m_{kj} S_j - m_{jk} S_k), \\ f_{2k} = \beta_{1k} S_k f_k(I_k) + \beta_{2k} S_k g_k(E_k) - \epsilon_k E_k + \sum_{j=1}^{n} (n_{kj} E_j - n_{jk} E_k), \\ f_{3k} = \epsilon_k E_k - \delta_k I_k + \sum_{j=1}^{n} (p_{kj} I_j - p_{jk} I_k), \\ f_{4k} = \delta_k I_k - (\lambda_k + \kappa_k) H_k, \\ f_{5k} = \lambda_k H_k + \sum_{j=1}^{n} (q_{kj} R_j - q_{jk} R_k). \end{cases}$$

It is obvious that $F_k = (f_{1k}, f_{2k}, f_{3k}, f_{4k}, f_{5k})$ satisfies the local Lipschitz condition about $(S_k, E_k, I_k, H_k, R_k)$, then system (3) has a unique solution. Next, the nonnegative solution will be analyzed. Consider the following auxiliary system:

$$\begin{cases} {}_0^C D_t^\alpha \underline{S}_k = -\beta_{1k} \underline{S}_k f_k(\underline{I}_k) - \beta_{2k} \underline{S}_k g_k(\underline{E}_k) - \rho_k \underline{S}_k \\ \qquad + \sum_{j=1}^{n} (m_{kj} \underline{S}_j - m_{jk} \underline{S}_k), \\ {}_0^C D_t^\alpha \underline{E}_k = \beta_{1k} \underline{S}_k f_k(\underline{I}_k) + \beta_{2k} \underline{S}_k g_k(\underline{I}_k) - \epsilon_k \underline{E}_k \\ \qquad + \sum_{j=1}^{n} (n_{kj} \underline{E}_j - n_{jk} \underline{E}_k), \\ {}_0^C D_t^\alpha \underline{I}_k = \epsilon_k \underline{E}_k - \delta_k \underline{I}_k + \sum_{j=1}^{n} (p_{kj} \underline{I}_j - p_{jk} \underline{I}_k), \\ {}_0^C D_t^\alpha \underline{H}_k = \delta_k \underline{I}_k - (\lambda_k + \kappa_k) \underline{H}_k, \\ {}_0^C D_t^\alpha \underline{R}_k = \lambda_k \underline{H}_k + \sum_{j=1}^{n} (q_{kj} \underline{R}_j - q_{jk} \underline{R}_k), \\ \underline{S}_k(0) = \underline{E}_k(0) = \underline{I}_k(0) = \underline{H}_k(0) = \underline{R}_k(0) = 0. \end{cases}$$

Through the comparison theorem, it is not difficult to find that the following auxiliary system has a unique solution $(0, 0, 0, 0, 0)$. Then the following equation holds:

$$(S_k, E_k, I_k, H_k, R_k) > (0, 0, 0, 0, 0).$$

Next, adding all equations gives ${}_0^C D_t^\alpha N \leq \Lambda - \rho N$ where $N = \sum_{j=1}^{n} (S_j + E_j + I_j + H_j + R_j + D_j)$, $\Lambda = \sum_{j=1}^{n} \Lambda_j$ and $\rho = \min\{\rho_1, \rho_2, \ldots, \rho_n\}$. Then

$$N(t) \leq (N(0) - \frac{\Lambda}{\rho}) E_\alpha(-\rho t^\alpha) + \frac{\Lambda}{\rho}.$$

Therefore, the region Ω is positively invariant for system (3). □

3.2. Local stability

The exploration of the existence and local stability of the disease-free equilibrium point is the focus of this section.

Theorem 3.2. *There are a unique disease-free equilibrium point* $E^0 = (S_1^*, 0, 0, 0, 0, \ldots, S_n^*, 0, 0, 0, 0)$ *for system* (3) *where* $S^* = (S_1^*, \ldots, S_n^*)$, $S^* = A^{-1}\Lambda$, $\Lambda = (\Lambda_1, \ldots, \Lambda_n)$ *and*

$$A = \begin{pmatrix} \rho_1 + \sum_{j\neq 1}^{n} m_{j1} & -m_{12} & \cdots & -m_{1n} \\ -m_{21} & \rho_2 + \sum_{j\neq 2}^{n} m_{j2} & \cdots & -m_{2n} \\ \vdots & \vdots & \vdots & \vdots \\ -m_{n1} & -m_{n2} & \cdots & \rho_2 + \sum_{j\neq n}^{n} m_{jn} \end{pmatrix}.$$

Proof. Obviously, E^0 satisfies the following equation:

$$\Lambda_k - \rho_k S_k^* + \sum_{j=1}^{n}(m_{kj}S_j^* - m_{jk}S_k^*) = 0,$$

then the above equation can be written as the following matrix form:

$$AS^* = \Lambda.$$

It can be found that the matrix A is strictly diagonally dominant, and then it follows from [36] that one has $A^{-1} \geq 0$. So according to [37], there exists a unique solution $S^* = A^{-1}\Lambda$. Therefore, there exists a unique disease-free equilibrium point E^0 of system (3). □

The predicted number of secondary cases, which a typical infectious individual should create in a community that is totally susceptible, is known as the basic reproduction number R_0. According to Watmough et al. [38], it can be determined that an infectious disease can commonly infect the community if one diseased individual can typically infect more than one susceptible individual when $R_0 \geq 1$. On the other hand, if $R_0 < 1$, each infected individual produces less than one new infection, and the infectious diseases cannot grow. Thus, it is very important to describe the relationship between the basic reproduction number and the spread of infectious diseases. Here, the basic reproduction number R_0 is stated as follows.

Theorem 3.3. *Under hypothesis* ***H****, the basic reproduction number* R_0 *is*

$$R_0 = \rho(F_{11}V_{11}^{-1} - F_{12}V_{11}^{-1}V_{21}V_{22}^{-1}),$$

where matrixes $F_{11} = diag(\beta_{21}b_1S_1, \ldots, \beta_{2n}b_nS_n)$, $F_{12} = diag(\beta_{11}a_1S_1, \ldots, \beta_{1n}a_nS_n)$, $V_{21} = diag(-\epsilon_1, \ldots, -\epsilon_n)$,

$$V_{11} = \begin{pmatrix} \epsilon_1 + \sum_{j\neq 1}^{n} n_{1j} & -n_{12} & \cdots & -n_{1n} \\ -n_{21} & \epsilon_2 + \sum_{j\neq 2}^{n} n_{2j} & \cdots & -n_{2n} \\ \vdots & \vdots & \vdots & \vdots \\ -n_{n1} & -n_{n2} & \cdots & \epsilon_n + \sum_{j\neq n}^{n} n_{nj} \end{pmatrix},$$

and

$$V_{22} = \begin{pmatrix} \delta_1 + \sum_{j\neq 1}^{n} p_{1j} & -p_{12} & \cdots & -p_{1n} \\ -p_{21} & \delta_2 + \sum_{j\neq 2}^{n} p_{2j} & \cdots & -p_{2n} \\ \vdots & \vdots & \vdots & \vdots \\ -p_{n1} & -p_{n2} & \cdots & \delta_n + \sum_{j\neq n}^{n} p_{nj} \end{pmatrix}.$$

Proof. Let consider the following matrixes:

$$F_0 = \begin{pmatrix} \beta_{11}S_1f_1(I_1) + \beta_{21}S_1g_k(E_1) \\ \vdots \\ \beta_{1n}S_nf_n(I_n) + \beta_{2n}S_ng_n(E_n) \\ 0 \\ \vdots \\ 0 \\ 0 \\ \vdots \\ 0 \end{pmatrix} \text{ and}$$

$$V_0 = \begin{pmatrix} \epsilon_1E_1 - \sum_{j=1}^{n}(n_{1j}E_j - n_{j1}E_1) \\ \vdots \\ \epsilon_nE_n - \sum_{j=n}^{n}(n_{nj}E_j - n_{jn}E_n) \\ -\epsilon_1E_1 + \delta_1I_1 - \sum_{j=1}^{n}(p_{1j}I_j - p_{j1}I_1) \\ \vdots \\ -\epsilon_nE_n + \delta_nI_n - \sum_{j=n}^{n}(p_{nj}I_j - p_{jn}I_n) \\ -\delta_1I_1 + (\lambda_1 + \kappa_1)H_1 \\ \vdots \\ -\delta_1I_n + (\lambda_n + \kappa_n)H_n \end{pmatrix}.$$

Let $u = (E_1, \ldots, E_n, I_1, \ldots, I_n, H_1, \ldots, H_n)$, then take the derivative of F_0 and V_0 for u at the disease-free equilibrium point E^0, respectively, we can see as follows:

$$F = \begin{pmatrix} F_{11} & F_{12} & 0 \\ 0 & 0 & 0 \\ 0 & 0 & 0 \end{pmatrix} \text{ and } V = \begin{pmatrix} V_{11} & 0 & 0 \\ V_{21} & V_{22} & 0 \\ 0 & V_{32} & V_{33} \end{pmatrix},$$

where $F_{11} = diag(\beta_{21}b_1S_1^*, \ldots, \beta_{2n}b_nS_n^*)$, $F_{12} = diag(\beta_{11}a_1S_1^*, \ldots, \beta_{1n}a_nS_n^*)$, $V_{21} = diag(-\epsilon_1, \ldots, -\epsilon_n)$, $V_{33} = diag((\lambda_1 + \kappa_1), \ldots, (\lambda_n + \kappa_n))$, $V_{32} = diag\ (-\delta_1, \ldots, -\delta_n)$,

$$V_{11} = \begin{pmatrix} \epsilon_1 + \sum_{j\neq 1}^{n} n_{1j} & -n_{12} & \cdots & -n_{1n} \\ -n_{21} & \epsilon_2 + \sum_{j\neq 2}^{n} n_{2j} & \cdots & -n_{2n} \\ \vdots & \vdots & \vdots & \vdots \\ -n_{n1} & -n_{n2} & \cdots & \epsilon_n + \sum_{j\neq n}^{n} n_{nj} \end{pmatrix},$$

and

$$V_{22}=\begin{pmatrix} \delta_1+\sum_{j\neq 1}^{n} p_{1j} & -p_{12} & \cdots & -p_{1n} \\ -p_{21} & \delta_2+\sum_{j\neq 2}^{n} p_{2j} & \cdots & -p_{2n} \\ \vdots & \vdots & \vdots & \vdots \\ -p_{n1} & -p_{n2} & \cdots & \delta_n+\sum_{j\neq n}^{n} p_{nj} \end{pmatrix}.$$

Then according to [39], the basic reproduction number is as follows:

$$R_0=\rho(FV^{-1})=\rho(F_{11}V_{11}^{-1}-F_{12}V_{11}^{-1}V_{21}V_{22}^{-1}),$$

where $\rho(F_{11}V_{11}^{-1}-F_{12}V_{11}^{-1}V_{21}V_{22}^{-1})$ is the spectral radius of the matrix $(F_{11}V_{11}^{-1}-F_{12}V_{11}^{-1}V_{21}V_{22}^{-1})$. □

Remark 3.1. According to [40], the epidemic size $\varsigma_k=S_k(0)-S_k^*$ of city k is defined as the number of individuals affected by the infectious disease, where $S_k(0)$ is initial condition and S_k^* is the disease-free equilibrium point of susceptible individuals within city k.

Remark 3.2. When individual migration is not taken into consideration, it can be calculated from [10] that the basic reproduction number R_{0u}^k of city k is

$$R_{0u}^k=S_k^*\left(\frac{\beta_{2k}b_k}{\epsilon_k}+\frac{\beta_{1k}a_k}{\delta_k}\right).$$

Remark 3.3. When individual migration is taken into consideration, R_0^k of city k is

$$R_0^k=\frac{S_k^*}{\epsilon_k+\sum_{j\neq k}^{n} n_{kj}}\left(\beta_{2k}b_k+\frac{\beta_{1k}a_k\epsilon_k}{\delta_k+\sum_{j\neq k}^{n} p_{kj}}\right).$$

Remark 3.4. It is easy to see that R_0^k are not dependent on λ_k, κ_k and m_{kj}. Like [41], the other Λ_k, β_{1k}, β_{2k}, ρ_k, ϵ_k, n_{kj}, p_{kj} and δ_k are calculated as follows:

$$A_{\Lambda_k}=\frac{\Lambda_k}{R_0^k}\frac{\partial R_0^k}{\partial \Lambda_k}=1,\quad A_{\rho_k}=\frac{\rho_k}{R_0^k}\frac{\partial R_0^k}{\partial \rho_k}=-1,$$

$$A_{\beta_{1k}}=\frac{\beta_{1k}}{R_0^k}\frac{\partial R_0^k}{\partial \beta_{1k}}=\frac{\frac{\beta_{1k}a_k\epsilon_k}{\delta_k+\sum_{j\neq k}^{n} p_{kj}}}{\beta_{2k}b_k+\frac{\beta_{1k}a_k\epsilon_k}{\delta_k+\sum_{j\neq k}^{n} p_{kj}}},$$

$$A_{\beta_{2k}}=\frac{\beta_{2k}}{R_0^k}\frac{\partial R_0^k}{\partial \beta_{2k}}=\frac{\beta_{2k}b_k}{\beta_{2k}b_k+\frac{\beta_{1k}a_k\epsilon_k}{\delta_k+\sum_{j\neq k}^{n} p_{kj}}},$$

$$A_{\delta_k}=\frac{\delta_k}{R_0^k}\frac{\partial R_0^k}{\partial \delta_k}=-\frac{1}{(\delta_k+\sum_{j\neq k}^{n} p_{kj}^2)(\beta_{2k}b_k+\frac{\beta_{1k}a_k\epsilon_k}{\delta_k+\sum_{j\neq k}^{n} p_{kj}})},$$

$$A_{\epsilon_k}=\frac{\epsilon_k}{R_0^k}\frac{\partial R_0^k}{\partial \epsilon_k}=-\frac{1}{\epsilon_k+\sum_{j\neq k}^{n} n_{kj}}\left(\beta_{2k}b_k+\frac{\epsilon_k+\sum_{j\neq k}^{n} n_{kj}}{\delta_k+\sum_{j\neq k}^{n} p_{kj}}\right),$$

$$A_{n_{kj}}=\frac{n_{kj}}{R_0^k}\frac{\partial R_0^k}{\partial n_{kj}}=-1,$$

$$A_{p_{kj}}=\frac{p_{kj}}{R_0^k}\frac{\partial R_0^k}{\partial p_{kj}}=-\frac{1}{(\delta_k+\sum_{j\neq k}^{n} p_{kj}^2)(\beta_{2k}b_k+\frac{\beta_{1k}a_k\epsilon_k}{\delta_k+\sum_{j\neq k}^{n} p_{kj}})},$$

where A_{Λ_k}, A_{ρ_k}, $A_{\beta_{1k}}$, $A_{\beta_{2k}}$, A_{δ_k}, A_{ϵ_k}, $A_{n_{kj}}$ and $A_{p_{kj}}$ represent the normalized sensitivity on Λ_k, ρ_k, β_{1k}, β_{2k}, δ_k, ϵ_k, n_{kj} and p_{kj}, respectively. Through the above calculation found that the increase on Λ_k, β_{1k} and β_{2k} leads to the increase on R_0^k, but the increase on ρ_k, δ_k, ϵ_k, n_{kj} and p_{kj} leads to the decrease on R_0^k. In addition, the movement of susceptible individuals has no impact of R_0^k, but the movement of exposed and infected individuals is negatively correlated with R_0^k, and the movement of exposed individuals is more likely to influence the spread of the infectious disease with $|A_{n_{kj}}|>|A_{p_{kj}}|$.

Theorem 3.4. *Under hypothesis **H**, system (3) is locally asymptotically stable at the disease-free equilibrium point E^0 if $|arg(s_{F-V})|>\frac{\alpha\pi}{2}$.*

Proof. The following Jacobian matrix at the disease-free equilibrium point E^0 is considered:

$$J_{E^0}=\begin{pmatrix} J_{11} & * & 0 \\ 0 & F-V & 0 \\ 0 & * & J_{33} \end{pmatrix},$$

where matrixes

$$J_{11}=\begin{pmatrix} -\rho_1-\sum_{j=1}^{n} m_{j1} & m_{12} & \cdots & m_{1n} \\ m_{21} & -\rho_2-\sum_{j=1}^{n} m_{j2} & \cdots & m_{2n} \\ \vdots & \vdots & \vdots & \vdots \\ m_{n1} & m_{n2} & \cdots & -\rho_n-\sum_{j=1}^{n} m_{jn} \end{pmatrix},$$

$$J_{33}=\begin{pmatrix} -\sum_{j=1}^{n} q_{j1} & q_{12} & \cdots & q_{1n} \\ q_{21} & -\sum_{j=1}^{n} q_{j2} & \cdots & q_{2n} \\ \vdots & \vdots & \vdots & \vdots \\ q_{n1} & q_{n2} & \cdots & -\sum_{j=1}^{n} q_{jn} \end{pmatrix},$$

F and V see Theorem 3.3. Then if all eigenvalues of the Jacobian matrix J_{E^0} satisfy $|arg(s_i)|>\frac{\alpha\pi}{2}$, E^0 is locally asymptotically stable and unstable if for some eigenvalues s_i, $|arg(s_i)|\leq\frac{\alpha\pi}{2}$. Obviously, J_{11} and J_{33} are a nonsingular M-matrix, so J_{11} and J_{33} has all eigenvalues with negative real parts according to [42]. Consequently the local stability of E^0 depends only on eigenvalues of $F-V$. Thus, if all eigenvalues of $F-V$ satisfy $|arg(s_{F-V})|>\frac{\alpha\pi}{2}$, system (3) is locally asymptotically stable. □

Remark 3.5. If all the eigenvalues of $F-V$ are negative, that is $|arg(s_{F-V})|=\pi>\frac{\alpha\pi}{2}$, system (3) is locally asymptotically stable. Meanwhile, it is obvious that

$$|arg(s_{F-V})|=\pi\Leftrightarrow s_{F-V}<0\Leftrightarrow\rho(FV^{-1})<1\Leftrightarrow R_0<1.$$

It can be yielded that if $R_0<1$, the disease-free equilibrium point E^0 is locally asymptotically stable of system (3).

3.3. Global asymptotic stability of the disease-free equilibrium

In this subsection, the global asymptotic stability of the disease-free equilibrium point E^0 is discussed firstly. Furthermore, the uniform persistence of system (3) is also considered.

Theorem 3.5. *Under hypothesis* ***(H)*** *and* $|arg(s_{F-V})| > \frac{\alpha\pi}{2}$, *the disease-free equilibrium point* E^0 *is globally asymptotically stable of system* (3).

Proof. We use a method similar to the one used in [43]. Firstly, the boundedness of the susceptible class will be analyzed. According to Theorem 3.1 and hypothesis **(H)**, we know S_k, E_k and I_k $(k = 1, 2, \ldots, n)$ are nonnegative, thus one has

$$\begin{aligned} {}_0^C D_t^\alpha S_k &= \Lambda_k - \beta_{1k} S_k f_k(I_k) - \beta_{2k} S_k g_k(E_k) - \rho_k S_k \\ &\quad + \sum_{j=1}^{n} (m_{kj} S_j - m_{jk} S_k) \\ &\leq \Lambda_k - \rho_k S_k + \sum_{j=1}^{n} (m_{kj} S_j - m_{jk} S_k). \end{aligned} \tag{5}$$

Let $S = (S_1, \ldots, S_n)$, $S^* = (S_1^*, \ldots, S_n^*)$, $\Lambda = (\Lambda_1, \ldots, \Lambda_n)$ and

$$A = \begin{pmatrix} \rho_1 + \sum_{j\neq 1}^{n} m_{j1} & -m_{12} & \cdots & -m_{1n} \\ -m_{21} & \rho_2 + \sum_{j\neq 2}^{n} m_{j2} & \cdots & -m_{2n} \\ \vdots & \vdots & \vdots & \vdots \\ -m_{n1} & -m_{n2} & \cdots & \rho_2 + \sum_{j\neq n}^{n} m_{jn} \end{pmatrix},$$

then Eq. (5) can be written in the following matrix:

$${}_0^C D_t^\alpha S \leq \Lambda - AS = AS^* - AS,$$

so it is easy to see that the conclusion holds as follows:

$$S(t) \leq (S_0 - S^*) E_\alpha(-At^\alpha) + S^*.$$

Obviously, one has $S_k \leq S_k^*$. Next, the global stability of E_k, I_k and H_k will be discussed. Based on hypothesis **(H)**, one has $f_k(I_k) \leq a_k I_k$ and $g_k(E_k) \leq b_k E_k$. Then the following auxiliary system is considered:

$$\begin{cases} {}_0^C D_t^\alpha \overline{E_k} = \beta_{1k} S_k^* a_k \overline{I_k} + \beta_{2k} S_k^* b_k \overline{E_k} - \epsilon_k \overline{E_k} + \sum_{j=1}^{n} (n_{kj} \overline{E_j} - n_{jk} \overline{E_k}), \\ {}_0^C D_t^\alpha \overline{I_k} = \epsilon_k \overline{E_k} - \delta_k \overline{I_k} + \sum_{j=1}^{n} (p_{kj} \overline{I_j} - p_{jk} \overline{I_k}), \\ {}_0^C D_t^\alpha \overline{H_k} = \delta_k \overline{I_k} - (\lambda_k + \kappa_k) \overline{H_k}. \end{cases} \tag{6}$$

It is easy to see that

$${}_0^C D_t^\alpha W = (F - V) W, \tag{7}$$

where $W = (\overline{E}, \overline{I}, \overline{H})$, $\overline{E} = (\overline{E_1}, \ldots, \overline{E_n})$, $\overline{I} = (\overline{I_1}, \ldots, \overline{I_n})$, $\overline{H} = (\overline{H_1}, \ldots, \overline{H_n})$, F and V see Theorem 3.3. Thus, if $|arg(s_{F-V})| > \frac{\alpha\pi}{2}$, the above linear system (7) is locally asymptotically stable as well as globally asymptotically stable, that is

$$\lim_{t\to\infty} \overline{E}_k = \lim_{t\to\infty} \overline{I}_k = \lim_{t\to\infty} \overline{H}_k = 0.$$

According to the comparison theory and the nonnegative solution of E_k, I_k and H_k, one has

$$\lim_{t\to\infty} E_k = \lim_{t\to\infty} I_k = \lim_{t\to\infty} H_k = 0.$$

Based on the above analysis, when $t \to \infty$, one has

$${}_0^C D_t^\alpha S = AS^* - AS,$$

then one has

$$S(t) \to S^* \ (t \to \infty).$$

So E^0 is globally asymptotically stable if $|arg(s_{F-V})| > \frac{\alpha\pi}{2}$. □

Remark 3.6. Similar to Theorem 3.4, it can be concluded that if $R_0 < 1$, system (3) is globally asymptotically stable at the disease-free equilibrium point E^0.

Furthermore, the uniform persistence for system (3) is discussed in the following theorem.

Theorem 3.6. *Under hypothesis* ***(H)*** *and* $R_0 > 1$, *system* (3) *is uniformly persist, implying there exists a positive constant* δ *such that*

$$\liminf_{t\to+\infty} S_k \geq \delta, \ \liminf_{t\to+\infty} E_k \geq \delta,$$
$$\liminf_{t\to+\infty} I_k \geq \delta, \ \liminf_{t\to+\infty} H_k \geq \delta, \ \liminf_{t\to+\infty} R_k \geq \delta, \ 1 \leq k \leq n.$$

Proof. Let consider the following space:

$$\mathbb{X} = \mathbb{X}_1 \times \mathbb{X}_2 \times \cdots \times \mathbb{X}_n, \ \mathbb{X}^0 = \mathbb{X}_1^0 \times \mathbb{X}_2^0 \times \cdots \times \mathbb{X}_n^0,$$
$$\partial\mathbb{X} = \partial\mathbb{X}_1 \times \partial\mathbb{X}_2 \times \cdots \times \partial\mathbb{X}_n,$$

where $\mathbb{X}^0$ represents the interior of $\mathbb{X}$, $\partial\mathbb{X}$ denotes the boundary of $\mathbb{X}$ and

$$\mathbb{X}_k = \{(S_k, E_k, I_k, H_k, R_k) : S_k > 0, E_k \geq 0, I_k \geq 0, H_k \geq 0, R_k \geq 0\},$$

$$\mathbb{X}_k^0 = \{(S_k, E_k, I_k, H_k, R_k) : S_k > 0, E_k > 0, I_k > 0, H_k > 0, R_k > 0\},$$

$$\partial\mathbb{X}_k = \{(S_k, E_k, I_k, H_k, R_k) : S_k > 0, E_k = 0, I_k = 0, H_k = 0, R_k = 0\}.$$

Meanwhile, let $W(t) = (S_1, E_1, I_1, H_1, R_1, \ldots, S_n, E_n, I_n, H_n, R_n)$ be the solution of system (3) with initial value $W(0) = W_0 \in \mathbb{X}$, then $W(t) \in \mathbb{X}$ according to Theorem 3.1. For any $t \geq 0$, a continuous map $F(t) : \mathbb{X} \to \mathbb{X}$ is defined as follows:

$$F(t)W_0 = W(t).$$

In the following, the uniformly persistent of the map F will be analyzed based on Lemma 2.2. When $t = 0$, one has

$$F(0)W_0 = W(0),$$

this is $F(0) = I$ where I is the identity matrix. Meanwhile, it can be deduced that the following equation holds:

$$F(t+s)W_0 = W(t+s) = F(t)W(s) = F(t)F(s)W_0,$$

implying $F(0) = I$. Additionally, it is easy to see that $F(t)$ is C^0-semigroup on $\mathbb{X}$, point dissipative and compact in $\mathbb{X}$. Furthermore, consider the following system:

$${}_0^C D_t^\alpha S_k = \Lambda_k - \rho_k S_k + \sum_{j=1}^{n} (m_{kj} S_j - m_{jk} S_k).$$

According to Theorem 3.4, S_k^* is asymptotically stable, which finds that E^0 in $\partial\mathbb{X}$ is a global attractor of $F(t)$. Let

$$M = \{M_1\},$$

where $M_1 = \{E^0\}$. Because of $a_k = f_k'(0)$ and $b_k = g_k'(0)$, for all ϵ, there exists $\overline{\epsilon}$ that

$$f(\epsilon) > (a_k - \epsilon)\overline{\epsilon} \ \ and \ \ g(\epsilon) > (b_k - \epsilon)\overline{\epsilon}.$$

Let the stable set $W^s(E^0)$ of a compact invariant set E^0 defined by

$$W^s(E^0) = \{Y_0 \in \mathbb{X} : \omega(Y_0) \neq \emptyset, \omega(Y_0) \in E^0\},$$

where $\omega(Y_0)$ is ω-limit set through Y_0. System (3) has a solution $(S_k, E_k, I_k, H_k, R_k)$ when $W^s(E^0) \cap \mathbb{X}^0 \neq \emptyset$, implying $S_k \to 0$,

$E_k \to 0, I_k \to 0, H_k \to 0, R_k \to 0$ $(k = 1, 2, \ldots, n)$ as $t \to \infty$. So there exists a constant $\tau > 0$ such that $S_k > S_k^* - \epsilon$, $E_k > \epsilon$, $I_k > \epsilon$, $H_k > \epsilon$ and $R_k > \epsilon$ for $t \geq \tau$. Then according to the monotonicity of $f_k(I_k)$ and $g_k(E_k)$, one has

$$f(I_k) > f(\epsilon) > (a_k - \epsilon)\overline{\epsilon} \text{ and } g(E_k) > g(\epsilon) > (b_k - \epsilon)\overline{\epsilon}.$$

So the following auxiliary system is considered:

$$\begin{cases} {}_0^C D_t^\alpha \underline{E_k} = \beta_{1k} S_k^* (a_k - \epsilon)\overline{\epsilon}\underline{I_k} + \beta_{2k} S_k^* (b_k - \epsilon)\overline{\epsilon}\underline{E_k} - \epsilon_k \underline{E_k} \\ \qquad + \sum_{j=1}^{n} (n_{kj}\underline{E_j} - n_{jk}\underline{E_k}), \\ {}_0^C D_t^\alpha \underline{I_k} = \epsilon_k \underline{E_k} - \delta_k \underline{I_k} + \sum_{j=1}^{n} (p_{kj}\underline{I_j} - p_{jk}\underline{I_k}), \\ {}_0^C D_t^\alpha \underline{H_k} = \delta_k \underline{I_k} - (\lambda_k + \kappa_k)\underline{H_k}. \end{cases} \tag{8}$$

It is easy to see from system (8) that

$${}_0^C D_t^\alpha W = (F - V)(\overline{\epsilon}, \epsilon)W, \tag{9}$$

where $W = (\underline{E}, \underline{I}, \underline{H})$, $\underline{E} = (\underline{E_1}, \ldots, \underline{E_n})$, $\underline{I} = (\underline{I_1}, \ldots, \underline{I_n})$ and $\underline{H} = (\underline{H_1}, \ldots, \underline{H_n})$. Consider the basic reproduction number $R_0 > 1$, then one has

$$\rho(F_{11}V_{11}^{-1} - F_{12}V_{11}^{-1}V_{21}V_{22}^{-1})(\overline{\epsilon}, \epsilon) > 1,$$

which results in a contradiction with $E_k(t) \to 0$ $(t \to \infty)$. Hence one has $W^s(E^0) \cap \mathbb{X}^0 = \emptyset$, implying it is uniformly persistent at the operator $T(t)$, so system (3) is uniformly persistent if $R_0 > 1$. □

The existence of a positive equilibrium point is implied by the system (3)'s ultimate boundedenss and uniform persistence. As a result, we can derive the following theorem.

Theorem 3.7. *Under hypothesis* ***(H)*** *and* $R_0 > 1$, *there is at least one endemic equilibrium* $E^* = (S_1^*, E_1^*, I_1^*, H_1^*, R_1^*, \ldots, S_n^*, E_n^*, I_n^*, H_n^*, R_n^*)$ *of system* (3) *satisfying*

$$\begin{cases} \Lambda_k - \beta_{1k} S_k^* f_k(I_k^*) - \beta_{2k} S_k^* g_k(E_k^*) - \rho_k S_k^* \\ + \sum_{j=1}^{n} (m_{kj} S_j^* - m_{jk} S_k^*) = 0, \\ \beta_{1k} S_k^* f_k(I_k^*) + \beta_{2k} S_k^* g_k(E_k^*) - \epsilon_k E_k^* + \sum_{j=1}^{n} (n_{kj} E_j^* - n_{jk} E_k^*) = 0, \\ \epsilon_k E_k^* - \delta_k I_k^* + \sum_{j=1}^{n} (p_{kj} I_j^* - p_{jk} I_k^*) = 0, \\ \delta_k I_k^* - (\lambda_k - \kappa_k) H_k^* = 0, \\ \lambda_k H_k^* + \sum_{j=1}^{n} (q_{kj} R_j^* - q_{jk} R_k^*) = 0. \end{cases}$$

4. Numerical simulation

From the previous description, it is clear that E^0 is globally asymptotically stable when $R_0 < 1$ and conversely, system (3) is persistent, which can offer theoretical evidence for further COVID-19 prediction and control. Meanwhile, in order to analyze COVID-19 in different cities, this section is divided into two parts: no restrictions on individual migration and restrictions on individual migration. Furthermore, consider the corresponding integer-order model as follows:

$$\begin{cases} \frac{dS_k}{dt} = \Lambda_k - \beta_{1k} S_k f_k(I_k) - \beta_{2k} S_k g_k(E_k) - \rho_k S_k \\ \qquad + \sum_{j=1}^{n} (m_{kj} S_j - m_{jk} S_k), \\ \frac{dE_k}{dt} = \beta_{1k} S_k f_k(I_k) + \beta_{2k} S_k g_k(E_k) - \epsilon_k E_k + \sum_{j=1}^{n} (n_{kj} E_j - n_{jk} E_k), \\ \frac{dI_k}{dt} = \epsilon_k E_k - \delta_k I_k + \sum_{j=1}^{n} (p_{kj} I_j - p_{jk} I_k), \\ \frac{dH_k}{dt} = \delta_k I_k - (\lambda_k + \kappa_k) H_k, \\ \frac{dR_k}{dt} = \lambda_k H_k + \sum_{j=1}^{n} (q_{kj} R_j - q_{jk} R_k). \end{cases} \tag{10}$$

4.1. Data source

The Johns Hopkins University Center for System Science and Engineering provided the real data for this study [1]. Data on accumulated and confirmed cases, recovered cases, and death cases were shared by the Johns Hopkins University on January 23, 2020. Assuming that the confirmed individuals must be hospitalized, one has

$$\textit{Hospitalized} = \textit{Confirmed} - \textit{Recovered} - \textit{Death}.$$

Hence, we can get the real data of $H(t)$, $D(t)$ and $R(t)$ for different city from 23 January to 17 July, 2020.

4.2. The generalized incidence rate

As we know, Korobeinikov et al. [8] indicated that the stability of the endemic equilibrium point for infectious diseases is closely related to the concave of the incidence rate with respect to the infected individuals. Therefore, it is of practical significance to understand the role of different incidence rates in COVID-19. In this section, according to hypothesis **(H)**, the bilinear incidence rate and the saturation incidence rate are discussed as follows:

$$f_k(I_k) = I_k, \ g_k(E_k) = E_k.$$

$$f_k(I_k) = \frac{I_k}{1 + u_k I_k}, \ g_k(E_k) = \frac{E_k}{1 + v_k E_k}.$$

Meanwhile, as the public learns about COVID-19, the recovered rate and the disease-related mortality are time-varying rather than constant. Similar to [11], the best recovered rate λ_k and the best disease-related mortality κ_k are selected from the following equation:

$$\kappa_k = \begin{cases} \frac{p_1}{e^{p_2(t-p_3)} + e^{-p_2(t-p_3)}}, \\ p_1 e^{(p_2(t-p_3))^2}, \\ p_1 + e^{(p_2(t+p_3))}, \end{cases} \quad \text{and} \quad \lambda_k = \begin{cases} \frac{q_1}{1 + e^{-q_2(t-q_3)}}, \\ q_1 + e^{-q_2(t+q_3)}, \end{cases} \tag{11}$$

where q_i and q_i $(i = 1, 2, 3)$ are parameters for κ_k and λ_k, respectively. According to the real data reported by [2], the spread of COVID-19 in India and Brazil began on 30 January and 26 February, 2020, as the beginning of the outbreak of India and Brazil in this paper, respectively. According to Matlab function lsqcurvefit [11], the parameter identification results with system (3) and system (10) are depicted in Tables 1 and 2, respectively. Meanwhile, based on Tables 1 and 2, the five days forecast of India and Brazil are shown in Tables 3, 4, Figs. 2, 3, 4, 5, which the solid lines represent simulation results and circles represent real data. The results in Tables 1 and 2 show that the fractional-order

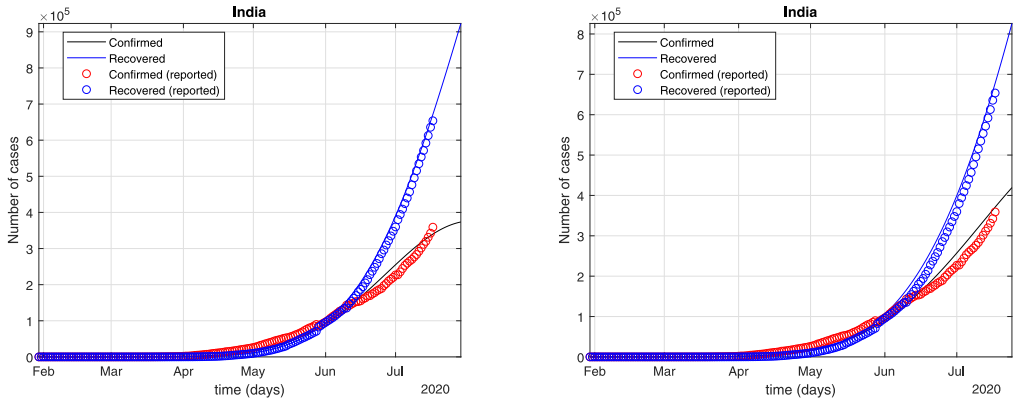

Fig. 2. The number of cases in India (Integer-order with the bilinear incidence rate (left), Fractional-order with the bilinear incidence rate (right)).

Table 1
Parameter identification of India.

India	Integer (Bilinear)	Fractional (Bilinear)	Integer (Saturation)	Fractional (Saturation)
Λ	0.3	0.6245	0.465	0.3
β_1	0.3869	1.206	1.156	2.358
β_2	0.5133	0.3079	0.3414	0.8
ϵ	0.0023	0.0555	0.0014	0.0692
ρ	0.0264	0.03	0.0188	0.0094
λ	$\frac{p_1}{1+e^{-p_2(t-p_3)}}$	$\frac{p_1}{1+e^{-p_2(t-p_3)}}$	$\frac{p_1}{1+e^{-p_2(t-p_3)}}$	$\frac{p_1}{1+e^{-p_2(t-p_3)}}$
κ	$b_1 e^{-q_2(t-q_3)^2}$	$q_1 e^{-q_2(t-q_3)^2}$	$q_1 e^{-q_2(t-q_3)^2}$	$q_1 e^{-q_2(t-q_3)^2}$

Table 2
Parameter identification of Brazil.

Brazil	Integer (Bilinear)	Fractional (Bilinear)	Integer (Saturation)	Fractional (Saturation)
Λ	0.3	0.5	0.8802	0.5189
β_1	1.839	1.082	0.2378	4.804
β_2	0.3733	0.928	0.4397	0.3
ϵ	0.0303	0.7905	0.1076	0.9609
ρ	0.0211	0.0214	0.0216	0.0431
δ	0.99	0.2434	0.3975	5.609×10^{-5}
λ	$\frac{p_1}{1+e^{-p_2(t-p_3)}}$	$\frac{p_1}{1+e^{-p_2(t-p_3)}}$	$\frac{p_1}{1+e^{-p_2(t-p_3)}}$	$\frac{p_1}{1+e^{-p_2(t-p_3)}}$
κ	$\frac{q_1}{e^{q_2(t-q_3)}}$	$\frac{q_1}{e^{q_2(t-q_3)}}$	$\frac{q_1}{e^{q_2(t-q_3)}}$	$\frac{q_1}{e^{q_2(t-q_3)}}$

Table 3
Estimate the number of confirmed cases within five days in India ($\times 10^5$).

India	18 Jul	19 Jul	20 Jul	21 Jul	22 Jul
Real data	3.735	3.906	4.027	4.113	4.263
Integer (bilinear incidence rate)	3.454	3.499	3.52	3.556	3.583
Fractional (bilinear incidence rate)	3.781	3.869	3.936	4.002	4.079
Integer (saturation incidence rate)	3.426	3.476	3.515	3.553	3.578
Fractional (saturation incidence rate)	3.645	3.696	3.741	3.792	3.815

system (3) can accurately forecast the real data in the upcoming week, with the real data of currently confirmed cases falling between 95% and 105% of the projected values.

4.3. Restrict individual migration

When individual movement is not considered, the parameters satisfy $m_{kj} = n_{kj} = p_{kj} = q_{kj} = 0$. Meanwhile, according to Section 4.2, the bilinear incidence rate is considered in this section. Then based on system (1), the following auxiliary system

Table 4
Estimate the number of confirmed cases within five days in Brazil ($\times 10^5$).

Brazil	18 Jul	19 Jul	20 Jul	21 Jul	22 Jul
Real data	5.487	5.598	5.242	5.228	5.528
Integer (bilinear incidence rate)	5.864	5.847	5.828	5.806	5.781
Fractional (bilinear incidence rate)	5.502	5.49	5.475	5.458	5.438
Integer (saturation incidence rate)	5.897	5.882	5.864	5.853	5.821
Fractional (saturation incidence rate)	5.857	5.844	5.819	5.793	5.769

is considered:

$$\begin{cases} {}_0^C D_t^\alpha S = \Lambda - \beta_1 SI - \beta_2 SE - \rho S, \\ {}_0^C D_t^\alpha E = \beta_1 SI + \beta_2 SE - \epsilon E, \\ {}_0^C D_t^\alpha I = \epsilon E - \delta I, \\ {}_0^C D_t^\alpha H = \delta I - (\lambda + \kappa) H, \\ {}_0^C D_t^\alpha R = \lambda H, \\ {}_0^C D_t^\alpha D = \kappa H. \end{cases} \tag{12}$$

4.3.1. Sensitivity analysis of parameters in R_{0u}^k

When individual movement is not taken into consideration in this section, Partial Rank Correlation Coefficients (PRCC) value and Latin hypercube sampling (LHS) [44], which are one of the Monte Carlo (MC) sampling methods established by Mckay in 1979 [45], can be used to account for the sensitivity of the parameter to the basic reproduction number. LHS has the advantage of using fewer iterations than other random sampling techniques and avoiding the clustering phenomenon of sampling [45]. In order to determine which aspects of a certain intervention have the greatest impact on how quickly a new infection spreads, it can be seen from Remark 3.4 that the parameters of system (12) all affect the basic reproduction number to varying degrees, thereby affecting the spread of the infectious disease. We perform LHS on the parameters that appear in R_{0u}^k. PRCC are calculated, and a total of 1000 simulations per LHS run are carried out. A uniform distribution is chose as the prior distribution when performing parameter sampling. The parameters Λ, ρ, ϵ, β_1, β_2 and δ of system (12) are set as input variables, and the basic reproduction number R_{0u}^k as the output. The specific process is as follows:
(1) There are six parameters that affect the change of R_{0u}^k, which are Λ, ρ, ϵ, β_1, β_2 and δ. Through LSH, [0, 1] is divided into 1000 simulations, and 6×1000 parameters are generated through random selection on each interval by a uniform distribution.
(2) Calculate the basic reproduction number R_{0u}^k for each parameter.

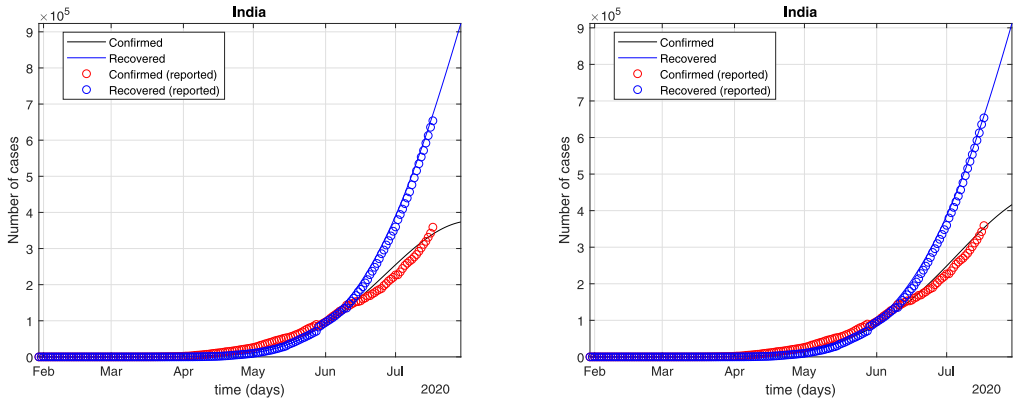

Fig. 3. The number of cases in India (Integer-order with the saturation incidence rate (left), Fractional-order with the saturation incidence rate (right)).

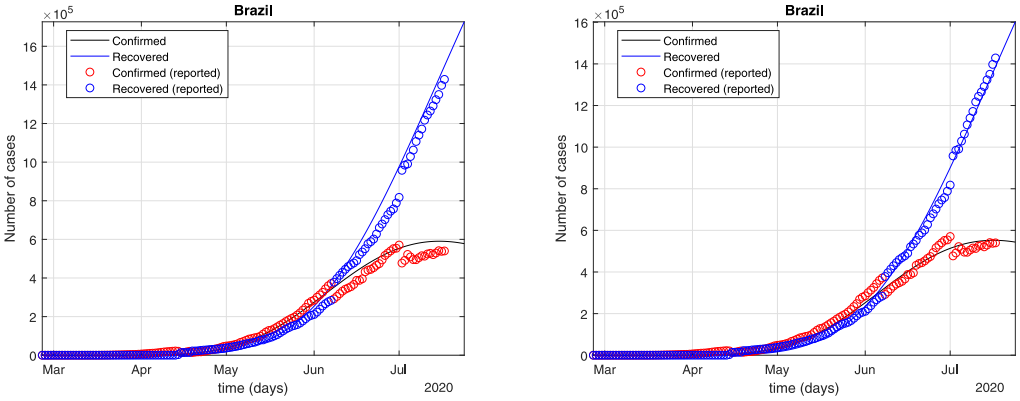

Fig. 4. The number of cases in Brazil (Integer-order with the bilinear incidence rate (left), Fractional-order with the bilinear incidence rate (right)).

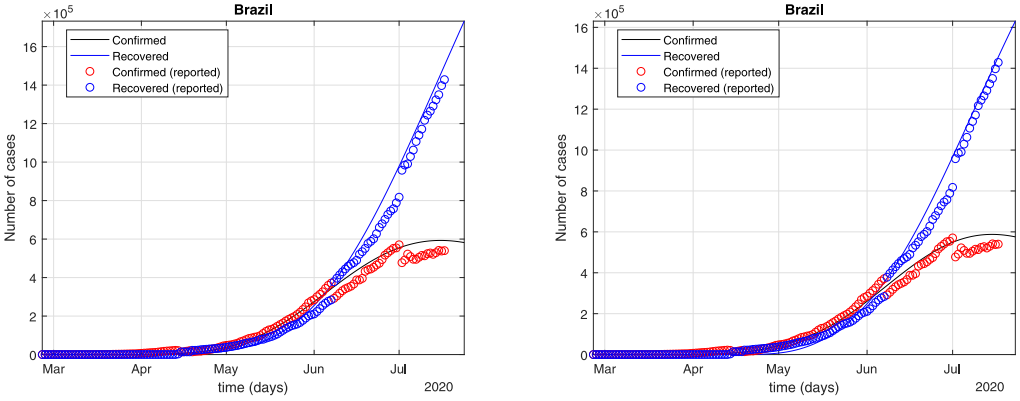

Fig. 5. The number of cases in Brazil (Integer-order with the saturation incidence rate (left), Fractional-order with the saturation incidence rate (right)).

(3) PRCC is calculated by Matlab function *partialcorr*.
(4) The PRCC's influence on the basic reproduction number R_{0u}^k can increase with increasing PRCC absolute value. However, it is believed that the parameter is not significant if the p value is greater than 0.05.

Table 5 lists the PRCC values of the six parameters associated with R_{0u}^k and Fig. 6 shows the histogram of PRCC value. From Table 5 and Fig. 6, the following conclusion holds:
(1) the parameters Λ, β_1 and β_2 have a positive influence on R_{0u}^k, but ρ, ϵ and δ have a negative influence, which is consistent with Remark 3.4;
(2) the positive impact of birth rate Λ is the most obvious with $PRCC(\Lambda) = 0.5868$;
(3) the positive impact of the transmission rate β_2 for the exposed population is more obvious than that of the infected population with $PRCC(\beta_2) > PRCC(\beta_1)$. That is, the greater the transmission coefficient of the exposed population, the greater the value of the basic reproduction number R_{0u}^k, and then the greater the number of people infected with COVID-19. Therefore, it is more critical to limit exposed individual. However, because exposed individual does not show any symptoms, identifying them is very difficult, which is a key reason for the spread of COVID-19;
(4) the diagnosis rate δ has more greater negative impact on R_{0u}^k. That is to say, enhancing nucleic acid detection can effectively reduce R_{0u}^i, thereby reducing the number of infected people;

Table 5
The PRCC values and p-value of the parameters with respect to R^k_{0u}.

Input	PRCC values	p-value
Λ	0.5868	0
ρ	−0.5363	0
ϵ	−0.1368	0
β_2	0.1035	3.5×10^{-6}
β_1	0.0847	1.448×10^{-4}
δ	−0.4362	0

(5) from the p-value, it can be found that the p-values of all parameters are less than 0.05, so they all have a significant impact on the basic reproduction number R^k_{0u}.

Therefore, based on the above analysis, it can be obtained that controlling the influx of foreign population and enhancing nucleic acid detection are the most effective measures to control COVID-19. Meanwhile, home isolation can also control COVID-19. Therefore, this evidence confirms the effectiveness of Chinese government's interruption policies, such as home isolation, prohibition of the inflow of foreign population, and enhancing nucleic acid detection, which may provide a good reference for the other countries.

4.3.2. China's second outbreak

From the analysis in Section 4.3.1, it can be found that enhancing the diagnosis rate and controlling the inflow of foreign population can effectively control the spread of the epidemic. For China, individual migration has been strictly restricted at the beginning of COVID-19. Therefore, the impact of enhanced diagnosis rate will be only considered in this section. Due to the increase in public awareness and the development of detection technology, the time from onset to diagnosis is gradually shortened. Additionally, despite the use of the nucleic acid test method, the number of confirmed cases climbed significantly and peaked in early February 2020 as a result of the use of the CT diagnosis method. As a result, it is assumed that starting on 12 February, 2020, China's diagnosis rate can reach and remain at its highest level. However, the third COVID-19 wave has been occurring in Beijing since the end of June 2020. Beijing has said that starting on 17 June, 2020, nucleic acid could be more readily detected. As a result, a new distribution, rather than the max level dated June 17, now governs the diagnostic rate. Similar to [46], the following piecewise function are described the diagnosed period of two and three peaks:

$$\frac{1}{\delta_k} = \begin{cases} (\frac{1}{\delta_0} - \frac{1}{\delta_e})e^{-w_1 t} + \frac{1}{\delta_e}, & t < t_1, \\ \frac{1}{\delta_e}, & t \geq t_1, \end{cases} \quad \text{and}$$

$$\frac{1}{\delta_k} = \begin{cases} (\frac{1}{\delta_0} - \frac{1}{\delta_e})e^{-w_1 t} + \frac{1}{\delta_e}, & t < t_1, \\ \frac{1}{\delta_e}, & t_1 \leq t \leq t_2, \\ (\frac{1}{\delta_e} - \frac{1}{\delta_f})e^{-w_2(t-t_2)} + \frac{1}{\delta_f}, & t > t_2, \end{cases} \tag{13}$$

where δ_0, δ_e ($\delta_e > \delta_0$), w_1, w_2 and δ_f are similar to [46], t_1 is 13 February, 2020, t_2 is 17 June, 2020. Meanwhile, similar to [11], the best recovered rate λ_k and the best disease-related mortality κ_k are selected from Eq. (11). Then system (12) and system (10) are solved by predictor–correctors scheme and least squares method [11] by the real data from 23 January to 17 July, which 17 March, 2020 is considered as the beginning of the emergency in Heilongjiang, Shanghai and Guangdong, and 17 June, 2020 are considered as the beginning of the emergency in Beijing, respectively. From Figs. 7 and 8, the fractional-order system (12) is found to fit the real data more accurately than the integer-order system (10) does and COVID-19 in Beijing, Shanghai reaches its highest peak in a short time but there may be fourth wave peak, however, Heilongjiang and Guangdong are only two peaks and the third wave of epidemic peaks will not occur in a short time (current policies remain unchanged). Therefore, under the condition of restricting the migration of individuals, the fractional system (12) can better simulate the multi-peak problem of COVID-19, and the strengthening of nucleic acid detection can predict the new wave in advance, which provides a theoretical basis for the control of the epidemic.

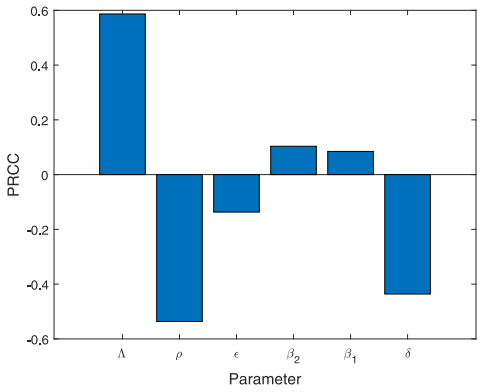

Fig. 6. The sensitivity analysis of R^k_{0u}.

4.4. Individual migration

As of 17 July, 2020, the United States has a total of 3,647,715 confirmed cases, 139266 deaths and 1,107,204 recovery cases. It is urgent to formulate reasonable and effective mitigation measures. Thus in this section, based on the sensitivity analysis of parameter to R^k_0, the effect mitigation measures are provided to control the development of COVID-19 in US.

4.4.1. Sensitivity analysis of parameters in R^k_0

Similar to Section 4.3.1, consider two cities to examine the sensitivity of parameters to R^k_0 ($k = 1, 2$). Then when $n = 2$, system (3) can be simplified as follows:

$$\begin{cases} {}^C_0D^\alpha_t S_1 = \Lambda_1 - \beta_{11}S_1I_1 - \beta_{21}S_1E_1 - \rho_1 S_1 + (m_{12}S_2 - m_{21}S_1), \\ {}^C_0D^\alpha_t E_1 = \beta_{11}S_1I_1 + \beta_{21}S_1E_1 - \epsilon_1 E_1 + (n_{12}E_2 - n_{21}E_2), \\ {}^C_0D^\alpha_t I_1 = \epsilon_1 E_1 - \delta_1 I_1 + (p_{12}I_2 - p_{21}I_1), \\ {}^C_0D^\alpha_t H_1 = \delta_1 I_1 - (\lambda_1 + \kappa_1)H_1, \\ {}^C_0D^\alpha_t R_1 = \lambda_1 H_1 + (q_{12}R_2 - q_{21}R_1), \\ {}^C_0D^\alpha_t S_2 = \Lambda_2 - \beta_{12}S_2I_2 - \beta_{22}S_2E_2 - \rho_2 S_2 + (m_{21}S_1 - m_{12}S_2), \\ {}^C_0D^\alpha_t E_2 = \beta_{12}S_1I_2 + \beta_{22}S_2E_2 - \epsilon_1 E_2 + (n_{21}E_1 - n_{12}E_1), \\ {}^C_0D^\alpha_t I_2 = \epsilon_2 E_2 - \delta_2 I_2 + (p_{21}I_1 - p_{12}I_2), \\ {}^C_0D^\alpha_t H_2 = \delta_2 I_2 - (\lambda_2 + \kappa_2)H_2, \\ {}^C_0D^\alpha_t R_2 = \lambda_2 H_2 + (q_{21}R_1 - q_{12}R_2). \end{cases} \tag{14}$$

It can be found from Remark 3.4 that there exists 16 parameter of the basic reproduction number R^k_0 ($k = 1, 2$), and then the 16 parameters are set as input variables, and R^k_0 as the output. Similar to Section 4.3.1, Table 6 lists the PRCC values and Fig. 9 shows the histogram of PRCC value. According to Table 6 and Fig. 9, it can be found that the following conclusion holds:
(1) the movement of susceptible individuals m_{kj} ($k, j = 1, 2$) does not affect R^k_0;
(2) the sensitivity of the parameter to R^k_0 ($k = 1, 2$) is same as that of Section 4.2.1, except for n_{12}, n_{21}, p_{12} and p_{21};

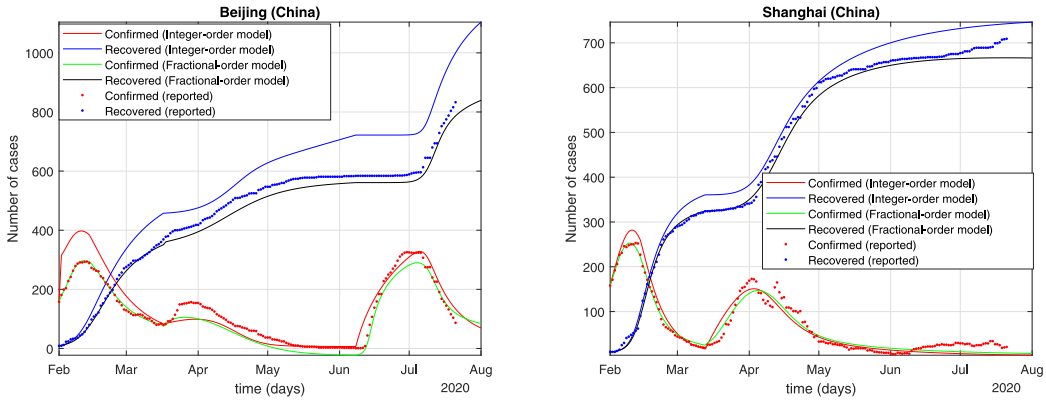

Fig. 7. The number of cases in Beijing and Shanghai.

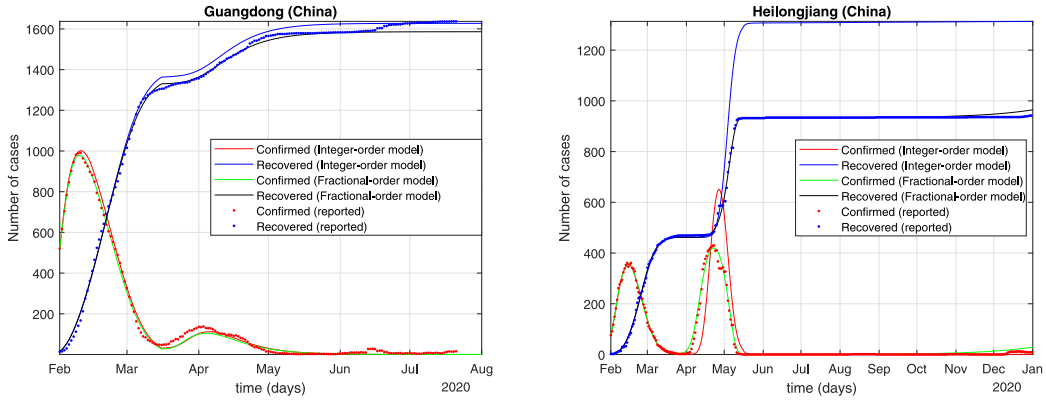

Fig. 8. The number of cases in Guangdong and Heilongjiang.

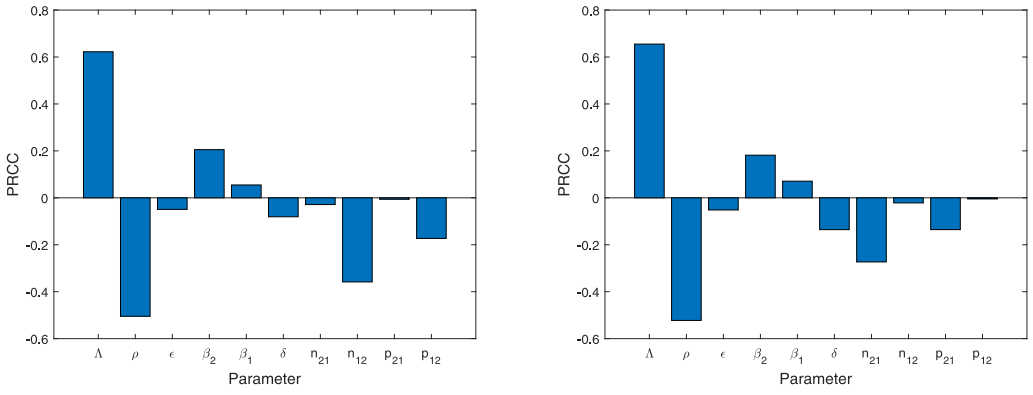

Fig. 9. The sensitivity analysis of R_0^1 (left) and R_0^2 (right).

(3) considering the basic reproduction number R_0^1 of city 1, the p-value of p_{21} is large than 0.05, which means that infected individuals migrating from city 1 have a significant impact on COVID-19 in city 1. But exposed and infected individuals migrating to city 1 have an impact on the spread of COVID-19 in city 1, and the impact of the inflow of exposed individuals is more significant because of $|PRCC(n_{12})| > |PRCC(p_{12})|$;
(4) contrary to the situation in city 1, the p-value of and p_{12} is large than 0.05, which means that infected individuals migrating from city 2 have a significant impact on the spread of disease in city 2. But exposed and infected individuals migrating from city 2 have an impact on the spread of COVID-19 in city 2, and the impact of the inflow of exposed individuals is more significant because of $|PRCC(n_{21})| > |PRCC(p_{21})|$.

Therefore, in order to alleviate the situation in severe areas of COVID-19, migration of exposed individuals must be strictly controlled.

4.4.2. US outbreak

In this subsection, the overall spread of COVID-19 in the US is considered first. Then system (10) and system (12) are solved by least squares method [11]. However, beginning 17 May, 2020, the number of confirmed individuals in the US had significantly increased. Emergency situations may have changed government regulations and people's attitudes, which led to an increase in the number of sick people. Therefore, it is assumed that the emergency starts on 17 May, and the outbreak's spread in the US is then examined in two stages as follows:
(1) 23 January–17 May, 2020;

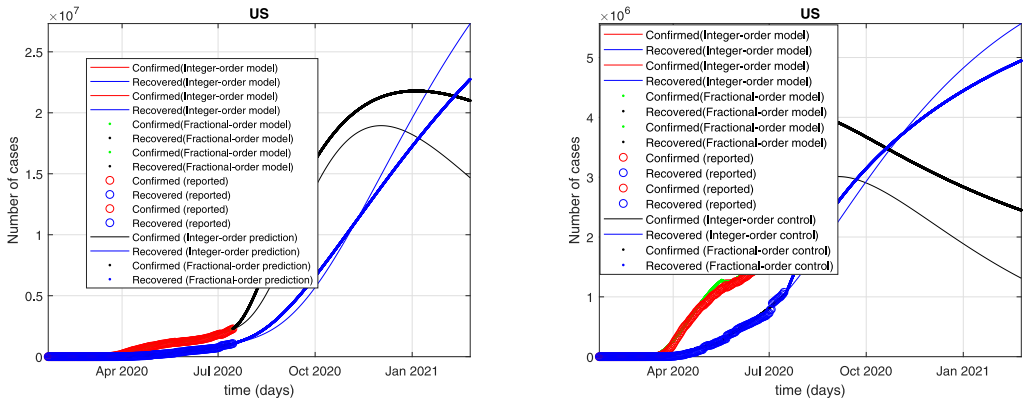

Fig. 10. The number of cases in US (without control (left), with control (right)).

Table 6
The PRCC values and p-value of the parameters with respect to R_0^1 (left) and R_0^2 (right).

Input	PRCC values	p-value
Λ_1	0.6513	0
ρ_1	−0.5294	0
ϵ_1	−0.0348	0.1194
β_{21}	0.1983	0
β_{11}	0.0564	0.0116
δ_1	−0.1427	0
n_{12}	−0.3584	0
n_{21}	−0.0286	0.2005
p_{12}	−0.1732	0
p_{21}	−0.0062	0.7806

Input	PRCC values	p-value
Λ_2	0.6496	0
ρ_2	−0.5223	0
ϵ_2	−0.0451	0.0435
β_{22}	0.1896	0
β_{12}	0.052	0.0153
δ_2	−0.1691	0
n_{12}	−0.0217	0.3318
n_{21}	−0.2732	0
p_{12}	−0.0048	0.8316
p_{21}	−0.1355	0

(2) 17 May–17 July, 2020.

Therefore, parameter identification is provided in Table 7 based on actual data from 23 January to 17 July 2020. From Fig. 10 and Table 8, it is clear that the fractional-order system (12) is capable of accurately forecasting the confirmed case for the upcoming week. In the meantime, Table 8 shows that, regardless of whether in the first stage or the second stage, the parameter findings of the fractional-order system and integer-order fitting are totally different.

Based on Remark 3.2, $R_{0u}^k = 49.84$ is very high. From the analysis in Section 4.2, it can be found that enhancing the diagnosis rate, reducing contact with infected people and controlling the inflow of foreign population can effectively control the spread of COVID-19. However, the United States is not currently doing anything to limit the influx of foreign population, so it is only considering enhancing nucleic acid testing and reducing contact with infected people to control COVID-19. Like [46], the diagnosed period $\frac{1}{\delta_k}$ of US are as follows:

$$\frac{1}{\delta(t)} = \begin{cases} \frac{1}{\delta_e}, & t \le t_3, \\ (\frac{1}{\delta_0} - \frac{1}{\delta_e})e^{-w(t-t_3)} + \frac{1}{\delta_e} & t > t_3. \end{cases} \tag{15}$$

The meaning of each symbol is similar to that in Section 4.3.2 (Eq. (13)). t_3 is 17 July, 2020, which mean increasing the diagnosis rate $\delta(t)$ from 17 July, 2020. At the same time, the contact rate β_i $(i = 1, 2)$ is limited by the number of hospitalizations like [46] as follows:

$$\beta_i(t) = \begin{cases} \beta_i, & logH(t) \le 1, \\ \frac{\beta_i}{logH(t)}, & logH(t) > 1. \end{cases} \tag{16}$$

It can be seen from Fig. 10 that increasing the diagnosis rate $\delta(t)$ and controlling the infection rate β_i $(i = 1, 2)$ can effectively contain COVID-19. Therefore, enhanced nucleic acid testing and limited contact with infected individuals are important to control COVID-19.

4.4.3. US with individual migration

This subsection considers the impact of individual migration on COVID-19. We need to preprocess the data to remove data that are less than 0.5% of the current maximum number of confirmed cases. Therefore, the real data after 3 April, 2020 are selected to identify the parameters of system (14). Similar to the analysis of Section 4.4.2, we consider 17 May, 2020 as the beginning of the emergency, and the COVID-19 spread in New York and Los Angeles into two phases:
(1) 3 April–17 May, 2020;
(2) 17 May-17 July, 2020.

Meanwhile, the recovered data of New York and Los Angeles have not been collected by [1], and then we take *hospitalized* + *recovered* individuals as a whole to conduct parameter identification and short-term prediction according to [11]. It can be found from Tables 9 and 10 and Fig. 11 that system (14) can better predict COVID-19. Meanwhile, it can be seen from Fig. 11 that the COVID-19 in New York has been peaked but not in Los Angles.

From the analysis of Section 4.4.1, we know that controlling the infection rate, improving the diagnosis rate and controlling the movement of exposed individuals have a significant effect on the control of COVID-19 in US. Therefore, similar to Section 4.4.2, the diagnosis rate δ_k and the migration rate n_{kj} are utilized as follows:

$$\frac{1}{\delta_k(t)} = \begin{cases} \frac{1}{\delta_e}, & t \le t_3, \\ (\frac{1}{\delta_0} - \frac{1}{\delta_e})e^{-w(t-t_3)} + \frac{1}{\delta_e}, & t > t_3, \end{cases} \quad and$$
$$n_{kj} = \begin{cases} n_{kj}, & log(H_k) < 1, \\ \frac{n_{kj}}{log(H_k)}, & log(H_k) \ge 1. \end{cases} \tag{17}$$

Meanwhile, the infection rate controlled by the number of hospitalizations is Eq. (16). From Fig. 12, we can seen the fractional-order system (14) with control (Eqs. (16) and (17)) in Los Angles can be control quickly but not in New York, which is still an open question and will be discussed later.

5. Conclusion

Based on individual migration, a fractional-order SEIHRDP model is proposed with the generalized incidence rate. Meanwhile, some results and effective mitigation measures is suggested to control COVID-19 as follows:
(1) The local and global asymptotic stability of the disease-free and endemic equilibrium points are investigated based on the basic reproduction number R_0.

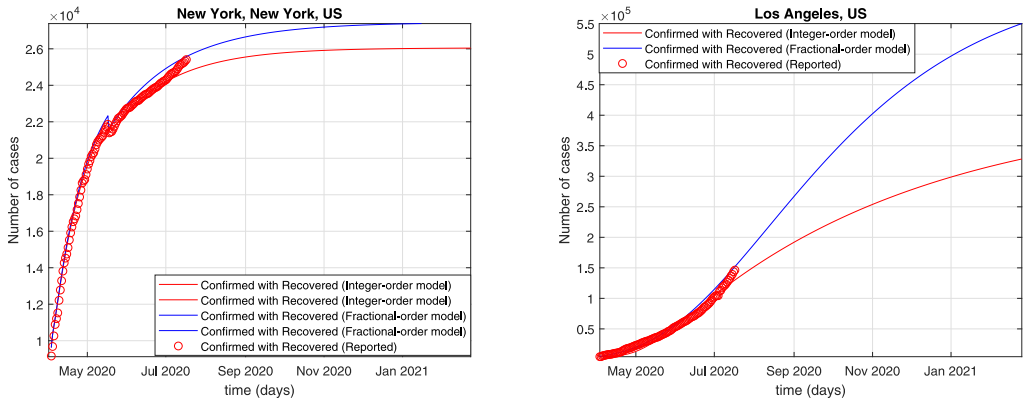

Fig. 11. The number of cases in New York and Los Angeles with individual migration.

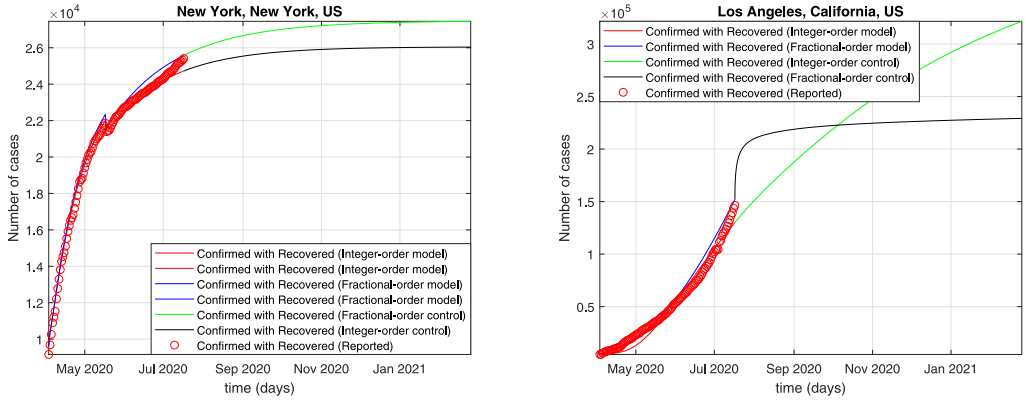

Fig. 12. The number of cases in New York and Los Angeles with control Eqs. (16) and (17).

Table 7
Parameter identification of US.

US	Integer (first stage)	Fractional (first stage)	Integer (second stage)	Fractional (second stage)
Λ	0.3	0.0935	0.3	0.4593
β_1	1.056	1.217	4.999	2.641
β_2	0.2969	0.4882	1.648×10^{-7}	3.724×10^{-7}
ϵ	0.1791	0.2876	0.0087	0.0077
ρ	0.0281	0.0497	0.0358	0.0272
δ	0.1243	0.2434	0.3975	0.205
λ	$p_1 + e^{-p_2(t+p_3)}$	$p_1 + e^{-p_2(t+p_3)}$	$p_1 + e^{-p_2(t+p_3)}$	$p_1 + e^{-p_2(t+p_3)}$
κ	$\frac{q_1}{e^{q_2(t-q_3)} + e^{-q_2(t-q_3)}}$	$\frac{q_1}{e^{q_2(t-q_3)} + e^{-q_2(t-q_3)}}$	$q_1 + e^{-q_2(t+q_3)}$	$q_1 + e^{-q_2(t+q_3)}$

Table 8
Estimate the number of confirmed cases within five days in US ($\times 10^6$).

Date	Real data	Fractional	Integer
18 July	2.449	2.503	2.397
19 July	2.502	2.541	2.425
20 July	2.534	2.578	2.454
21 July	2.575	2.616	2.482
22 July	2.617	2.655	2.511

Table 9
Estimate the number of confirmed cases within five days in New York ($\times 10^5$).

New York	18 Jul	19 Jul	20 Jul	21 Jul	22 Jul
Real data	1.977	1.98	1.983	1.987	1.99
Integer	1.978	1.979	1.98	1.981	1.981
Fractional	1.985	1.986	1.987	1.988	1.989

Table 10
Estimate the number of confirmed cases within five days in Los Angles ($\times 10^5$).

Los Angles	18 Jul	19 Jul	20 Jul	21 Jul	22 Jul
Real data	1.491	1.518	1.549	1.579	1.609
Integer	1.414	1.444	1.464	1.482	1.514
Fractional	1.494	1.517	1.547	1.579	1.608

(2) Based on the real data, it is found that the bilinear incidence rate has a better description of COVID-19 transmission than the saturation incidence rate. Therefore, the bilinear incidence rate is applied in modeling COVID-19. Meanwhile, this is the first time that looked at the impact of the incidence rate in the spread of COVID-19 using real data.

(3) By applying the value of PRCC, the sensitivity of the parameters to the basic reproduction number R_0^k and R_{0u}^k are obtained, which is consistent with Remark 3.4. Through the PRCC value, the diagnosis rate, the migration rate and the movement of the infected population are most sensitive to control COVID-19.

(4) Multiple peaks have been analyzed for COVID-19 and using four cities in China to show that the fractional-order system (1)

works well. Moreover, by increasing the diagnosis rate, it can be found that the third wave of epidemic in Beijing has reached its peak, but the arrival of the next wave of COVID-19 is not ruled out.
(5) Analyzing the situation in the United States, it can be seen that system (12) has better predictability than system (10). Meanwhile, by reducing the infection rate and increasing the diagnosis rate, the peak of the epidemic in the US can be accelerated.
(6) Results show that the fractional-order system can accurately forecast the real data in the upcoming week when taking into account individual migration between two cities. By limiting the movement of exposed individuals, raising the diagnosis rate, and lowering the infection rate, Los Angeles' peaks can appear and then decline immediately.

Furthermore, this study makes several contributions to predict multi-peak of COVID-19 in China and suggestions on controlling epidemic in the US by changing certain parameters. Nevertheless, this research raises some issues that require more investigation, including how medical and other factors affect the spread of infectious diseases, how to properly administer vaccines, how network topology affects disease transmission and so on.

Declaration of competing interest

The authors declare that they have no known competing financial interests or personal relationships that could have appeared to influence the work reported in this paper.

Acknowledgments

This work is supported by the Natural Science Foundation of Beijing Municipality, China [grant numbers Z180005], the National Nature Science Foundation of China [grant numbers 61772063] and the Fundamental Research Funds of the Central Universities, China [grant numbers 2020JBM074].

References

[1] The Johns Hopkins University Center for System Science and Engineering, Data of accumulated and newly confirmed cases, recovered case and death case of COVID-19, URL https://github.com/CSSEGISandData/COVID-19.
[2] Chan J, Yuan S, Kok K, To K, Chu H, Yang J, et al. A familial cluster of pneumonia associated with the 2019 novel coronavirus indicating person-to-person transmission: a study of a family cluster. Lancet 2020;395(10223):514–23.
[3] Huang C, Wang Y, Li X, Ren L, Zhao J, Hu Y, et al. Clinical features of patients infected with 2019 novel coronavirus in Wuhan, China. Lancet 2020;395(10223):497–506.
[4] Anderson R, Anderson B, May R. Infectious diseases of humans: Dynamics and control. Oxford University Press; 1992.
[5] Bailey N. The mathematical theory of infectious diseases and its applications. Charles Griffin Company Ltd; 1975.
[6] Upadhyay R, Pal A, Kumari S, Roy P. Dynamics of an SEIR epidemic model with nonlinear incidence and treatment rates. Nonlinear Dynam 2019;96(4):2351–68.
[7] Zou X, Wang K. Optimal harvesting for a stochastic regime-switching logistic diffusion system with jumps. Nonlinear Anal Hybrid 2014;13:32–44.
[8] Korobeinikov A, Maini P. Nonlinear incidence and stability of infectious disease models. Math Med Biol 2005;22(2):113–28.
[9] Peng L, Yang W, Zhang D, Zhuge C, Hong L. Epidemic analysis of COVID-19 in China by dynamical modeling. 2020, http://dx.doi.org/10.1101/2020.02.16.20023465, arXiv preprint arXiv:2002.06563.
[10] Xu C, Yu Y, Chen Y, Lu Z. Forecast analysis of the epidemics trend of COVID-19 in the USA by a generalized fractional-order SEIR model. Nonlinear Dynam 2020;101(3):1621–2634.
[11] Cheynet E. Generalized SEIR epidemic model (fitting and compution). GitHub; 2020, URL http://www.github.com/{ECheynet}/{SEIR}.
[12] Gao DZ, Cosner C, Cantrell RS, Beier JC, Ruan SG. Modeling the spatial spread of Rift Valley fever in Egypt. Bull Math Biol 2013;75(3):523–42.
[13] Phaijoo GR, Gurung DB. Mathematical study of dengue disease transmission in multi-patch environment. Appl Math 2016;7(14):1521–33.
[14] Eisenberg CM, Shuai ZS, Tien JH, den Driessche PV. A cholera model in a patchy environment with water and human movement. Math Biosci 2013;246(1):105–12.
[15] Julien A, Davis JR, David H, Richard J, Miller JM, den Driessche PV. A multi-species epidemic model with spatial dynamics. Math Med Biol 2005;(2):129–42.
[16] Cheng ZKJ, Shan J. 2019 Novel coronavirus: where we are and what we know. Infection 2021;49(197).
[17] Lu Z, Yu Y, Chen YQ, Ren G, Xu C, Wang S, et al. A fractional-order SEIHDR model for COVID-19 with inter-city networked coupling effects. Nonlinear Dynam 2020;101(3):1717–30.
[18] Smethurst D, Williams H. Are hospital waiting lists self-regulating? Nature 2001;410(6829):652–3.
[19] Meerschaert M, Sikorskii A. Stochastic models for fractional calculus. De Gruyter; 2011.
[20] Angstmann C, Henry B, Mcgann A. A fractional-order infectivity SIR model. Physica A 2016;86–93.
[21] Khan MA, Atangana A. Modeling the dynamics of novel coronavirus (2019-nCov) with fractional derivative. Alex Eng J 2020;59(4):2379–89.
[22] Chen Y, Cheng J, Jiang X, Xu X. The reconstruction and prediction algorithm of the fractional TDD for the local outbreak of COVID-19. 2020, arXiv preprint arXiv:2002.10302.
[23] Amjad SS, Najiroddin SI, Kottakkaran NS. A mathematical model of COVID-19 using fractional derivative: Outbreak in India with dynamics of transmission and control. Adv Differ Equ 2020;(373):1–19.
[24] Tang Z, Li XB, Li HQ. Prediction of new coronavirus infection based on a modified SEIR model. MedRxiv 2020. http://dx.doi.org/10.1101/2020.03.03.20030858.
[25] Zhou P, Ma J, Tang J. Clarify the physical process for fractional dynamical systems. Nonlinear Dynam 2020;1–12.
[26] Li H, Zhang L, Hu C, Jiang Y, Teng Z. Dynamical analysis of a fractional-order predator-prey model incorporating a prey refuge. J Appl Math Comput 2017;54(1–2):435–49.
[27] Singh J, Kumar D, Hammouch Z, Atangana A. A fractional epidemiological model for computer viruses pertaining to a new fractional derivative. Appl Math Comput 2018;316:504–15.
[28] Sierociuk D, Skovranek T, Macias M, Podlubny I, Petras I, Dzielinski A, et al. Diffusion process modeling by using fractional-order models. Appl Math Comput 2015;257:2–11.
[29] Podlubny I. Fractional differential equations. Academic Press; 1999.
[30] Li Y, Chen Y, Podlubny I. Mittag–Leffler stability of fractional order nonlinear dynamic systems. Automatica 2009;45(8):1965–9.
[31] Tang Q, Teng Z, Jiang H. Global behaviors for a class of multi-group SIRS epidemic models with nonlinear incidence rate. Taiwan J Math 2015;19(5):1509–32.
[32] Tang Z, Li X, Li H. Prediction of new coronavirus infection based on a modified SEIR model. Cold Spring Harbor Lab 2020;1–13.
[33] Lin M, Huang J, Ruan S, Yu P. Bifurcation analysis of an SIRS epidemic model with a generalized nonmonotone and saturated incidence rate. J Differ Equ 2019;267(3):1859–98.
[34] Muroya Y, Enatsu Y, Kuniya T. Global stability for a multi-group SIRS epidemic model with varying population sizes. Nonlinear Anal Real 2013;14(3):1693–704.
[35] Angstmann CN, Donnelly IC, Henry BI, Langlands T. Continuous-time random walks on networks with vertex- and time-dependent forcing. Phys Rev E 2013;88(2):022811.
[36] Li M, Graef JR, Wang LC, Karsai J. Global dynamics of a SEIR model with varying total population size. Math Biosci 1999;160(2):191–213.
[37] Kheiri H, Jafari M. Stability analysis of a fractional order model for the HIV/AIDS epidemic in a patchy environment. J Comput Appl Math 2018;323–39.
[38] van den Driessche P, Watmough J. Reproduction numbers and subthreshold endemic equilibria for compartmental models of disease transmission. Math Biosci 2002;180(1–2):29–48.
[39] Diekmann O, Heesterbeek J, Metz J. On the definition and the computation of the basic reproduction ratio R_0 in models for infectious diseases in heterogeneous populations. J Math Biol 1990;28(4):365–82.
[40] van den Driessche P, Watmough J. Heterogeneous social interactions and the COVID-19 lockdown outcome in a multi-group SEIR model. Math Model Nat Phenom 2020;15(36).
[41] Khajanchi S, Bera S, Roy TK. Mathematical analysis of the global dynamics of a HTLV-I infection model, considering the role of cytotoxic T-lymphocytes. Math Comput Simulat 2021;180.

[42] Berman A, Plemmons R. Nonnegative matrices in the mathematical sciences. Academic Press; 1979.
[43] Ruan SG, Wang WD, Levin SA. The effect of global travel on the spread of SARS. Math Biosci Eng 2012;3(1):205–18.
[44] Zhang K, Ji YP, Pan QW, Wei YM, Liu H. Sensitivity analysis and optimal treatment control for a mathematical model of Human Papillomavirus infection. AIMS Math 2020;5(5):2646–70.
[45] Huo HF, Feng LX. Global stability for an HIV/AIDS epidemic model with different latent stages and treatment. Appl Math Model 2013;37(3):1480–9.
[46] Tang B, Xia F, Tang S, Bragazzi N, Li Q, Sun X. The effectiveness of quarantine and isolation determine the trend of the COVID-19 epidemic in the final phase of the current outbreak in China. Int J Infect Dis 2020;96:636–47.